

Online Changepoint Detection via Dynamic Mode Decomposition

Victor K. Khamesi Niall M. Adams Dean A. Bodenham
Edward A. K. Cohen

Department of Mathematics, Imperial College London,
South Kensington Campus, London SW7 2AZ, U.K.
victor.khamesi21@imperial.ac.uk, n.adams@imperial.ac.uk,
dean.bodenham@imperial.ac.uk, e.cohen@imperial.ac.uk

Abstract

Detecting changes in data streams is a vital task in many applications. There is increasing interest in changepoint detection in the online setting, to enable real-time monitoring and support prompt responses and informed decision-making. Many approaches assume stationary sequences before encountering an abrupt change in the mean or variance. Notably less attention has focused on the challenging case where the monitored sequences exhibit trend, periodicity and seasonality. Dynamic mode decomposition is a data-driven dimensionality reduction technique that extracts the essential components of a dynamical system. We propose a changepoint detection method that leverages this technique to sequentially model the dynamics of a moving window of data and produce a low-rank reconstruction. A change is identified when there is a significant difference between this reconstruction and the observed data, and we provide theoretical justification for this approach. Extensive simulations demonstrate that our approach has superior detection performance compared to other methods for detecting small changes in mean, variance, periodicity, and second-order structure, among others, in data that exhibits seasonality. Results on real-world datasets also show excellent performance compared to contemporary approaches.

1 Introduction

Streaming data is ubiquitous in applications as diverse as cybersecurity [12], speech recognition [42], continual learning [45], finance [8], meteorology [32], biology [11], and medicine [40]. Detecting when the data generating mechanism changes is a crucial task in these applications. However, the time series data monitored in these applications often exhibit seasonality, such as higher values at certain times of the day, week, or year. Most changepoint detection methods are developed using the assumption that the data being analysed is piecewise-stationary. Such methods would be incapable of differentiating between changes in the distribution of the data and any seasonal effects.

In this paper, we propose a novel online changepoint detection method that can identify changepoints in streaming data while accounting for any seasonality in the time series. Our approach utilises a technique from dynamical systems called dynamic mode decomposition (DMD) [36, 37], which can decompose a p -dimensional time series into spatial *modes* and their associated *dynamics*, encapsulating their frequency and growth rate. Focusing on the $r < p$ dominant modes, this provides a low-rank factorisation of the time series used to construct a statistic which indicates whether or not a change has occurred. We demonstrate the effectiveness of this approach on simulated data with seasonality that have changes in mean, variance, periodicity, and second-order structure, and on several real-world datasets. The method has several advantages: it is nonparametric, so the type of change does not need to be specified in advance; it has few parameters and is shown experimentally to be robust to choices for these parameters; it is unsupervised and does not require offline training.

The rest of the paper is structured as follows: in Section 2, we describe background for changepoint detection and DMD; in Section 3, we introduce our novel method named **ChangePoint Detection via Dynamic Mode Decomposition (CPDMD)**; in Section 4, we show that CPDMD achieves state-of-the-art performance on both synthetic and real-world data; in Section 5, we briefly summarise our conclusions. The experiments on synthetic data focus on the case where the data is univariate and has a single change, since we are already considering several different types of changes, but the real-world experiments cover the case of multivariate data with multiple changepoints.

2 Background

We first provide an overview of the changepoint detection problem and dynamic mode decomposition algorithm to establish the necessary context and background.

2.1 Changepoint detection

Consider a stream of multivariate observations x_1, x_2, \dots where $x_t \in \mathbb{R}^p$, $p \in \mathbb{N}$, denotes the p -dimensional observation at regularly spaced and discrete time t , sampled from i.i.d. random variables X_1, X_2, \dots with changepoints τ_1, τ_2, \dots such that

$$\begin{aligned} X_1, X_2, \dots, X_{\tau_1} &\sim F_1, \\ X_{\tau_1+1}, X_{\tau_1+2}, \dots, X_{\tau_2} &\sim F_2, \\ X_{\tau_2+1}, X_{\tau_2+2}, \dots, X_{\tau_3} &\sim F_3, \text{ etc.}, \end{aligned}$$

where F_1, F_2, \dots is a sequence of *unknown* probability distributions such that $F_k \neq F_{k+1}$ for all $k \in \mathbb{N}$. Changepoint detection seeks to estimate the changepoint locations τ_1, τ_2, \dots . In other words, the problem consists in dividing the sequence of observations x_1, x_2, \dots into piecewise segments with the same data generation process. In the statistics and machine learning literature, changepoint detection is also referred to as distribution shift detection [31] or temporal segmentation [48]. While many approaches consider the *offline* setting [19, 39, 27], where the dataset is static and fully available, we are interested in the *online* setting, where observations are processed sequentially and changepoints need to be detected as soon as possible after occurring.

2.1.1 Related work

The changepoint literature is vast, so we only highlight a few notable approaches. Two early online approaches that are still widely used are CUSUM [29] and EWMA [33]. In recent years, an online Bayesian method [1] and its extensions (e.g. [20]) have become popular, although they can be computationally expensive for large sequences. Another class of approaches based on density ratio estimation includes KLIEP [41], uLSIF [15], and RuLSIF [52], with RuLSIF shown to have best performance among these three. Singular spectrum analysis has been adapted for changepoint detection in both univariate [28] and multivariate contexts [3]. Previous studies [43, 17] have considered using dynamic mode decomposition (DMD) for changepoint detection, although this was suggested as a secondary application after developing general DMD methodology, and only brief examples were provided without a comprehensive performance assessment.

2.2 Dynamic mode decomposition

Dynamic mode decomposition (DMD) [36, 21, 37] is a data-driven model reduction algorithm that aims to describe high-dimensional dynamical systems by discovering a low-dimensional subspace capturing dominant dynamics.

2.2.1 Continuous and discrete time

Continuous time. DMD assumes data is collected from an underlying dynamical system defined by $\frac{dx}{dt} = f(x, t; \theta)$ where $x(t) \in \mathbb{R}^p$ is the p -dimensional observation of the system's state at time t , θ contains the system's parameters, and $f : \mathbb{R}^p \times \mathbb{R} \rightarrow \mathbb{R}^p$ characterises the *unknown* dynamics. DMD linearly approximates the local dynamics using an operator $\mathcal{A} \in \mathbb{R}^{p \times p}$ such that $\frac{dx}{dt} \simeq \mathcal{A}x$. Given an initial condition $x(0)$, this differential equation has closed-form solution $x(t) = \sum_{j=1}^p \phi_j e^{\omega_j t} b_j$, where $\omega_j \in \mathbb{C}$ and $\phi_j \in \mathbb{C}^p$ are respectively the eigenvalues and eigenvectors of the matrix \mathcal{A} and $b_j \in \mathbb{C}$ are the coordinates of the initial condition $x(0)$ in the eigenvectors basis, for $j \in \{1, 2, \dots, p\}$.

Discrete time. In practice, one can only collect a discrete set of observations from the studied dynamical system. Therefore, DMD equations may be discretised considering equally time-spaced by Δt observations $x_k = x(k\Delta t) \in \mathbb{R}^p$, $k \in \mathbb{N}$, and the dynamical evolution is now described by $x_{k+1} = F(x_k)$ for some *unknown* function $F : \mathbb{R}^p \rightarrow \mathbb{R}^p$ representing the dynamics. Similar to continuous time, one may approximate the local dynamics such that $x_{k+1} \simeq Ax_k$, where $A = \exp(\mathcal{A}\Delta t) \in \mathbb{R}^{p \times p}$. The discretised system has solution $x_{k+1} = \sum_{j=1}^p \phi_j \lambda_j^k b_j$, where $\lambda_j \in \mathbb{C}$ and $\phi_j \in \mathbb{C}^p$ are respectively the eigenvalues (dynamics) and eigenvectors (modes) of the matrix A and $b_j \in \mathbb{C}$ are the coordinates of the initial condition x_1 in the eigenvectors basis, for $j \in \{1, 2, \dots, p\}$. The analogy between continuous and discrete time DMD is illustrated in Figure 1.

Computing the modes and dynamics. There are several approaches to extract the DMD modes and dynamics from a sequence of snapshots [36, 13, 37]. We use the standard

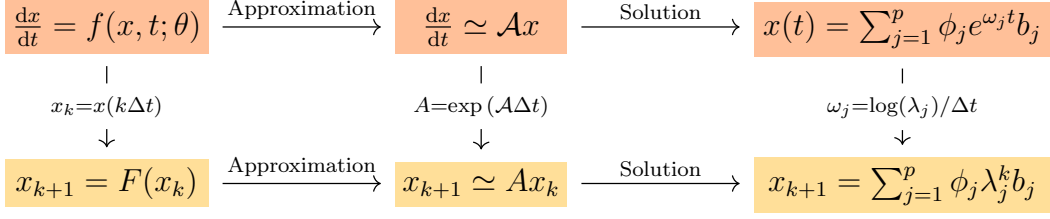


Figure 1: DMD analogy between continuous time (top) and discrete time (bottom) settings.

approach from [36], which relies on singular value decomposition; details are provided in Appendix B.1.

3 Proposed changepoint detection algorithm

We start by describing our approach to using dynamic mode decomposition (DMD) to extract the dynamics from a multivariate stream, then used to construct a statistic which reflects changes.

3.1 Space-time transformation of the data

Consider a time series x_1, x_2, \dots where $x_t = \begin{bmatrix} x_t^{(1)} & x_t^{(2)} & \dots & x_t^{(p)} \end{bmatrix}^\top \in \mathbb{R}^p$ denotes the p -dimensional observation at time $t \in \mathbb{N}$, $p \in \mathbb{N}$. Given a fixed window length $w \in \mathbb{N}$, let

$$X_t := [x_{t-w+1}, x_{t-w+2}, \dots, x_t] = \begin{bmatrix} x_{t-w+1}^{(1)} & x_{t-w+2}^{(1)} & \dots & x_t^{(1)} \\ x_{t-w+1}^{(2)} & x_{t-w+2}^{(2)} & \dots & x_t^{(2)} \\ \vdots & \vdots & \ddots & \vdots \\ x_{t-w+1}^{(p)} & x_{t-w+2}^{(p)} & \dots & x_t^{(p)} \end{bmatrix} := \begin{bmatrix} X_t^{(1)} \\ X_t^{(2)} \\ \vdots \\ X_t^{(p)} \end{bmatrix} \quad (1)$$

denote the concatenation of the last w snapshots at time t , reflecting the dynamics of the signal within this context window, where $X_t^{(j)} := \begin{bmatrix} x_{t-w+1}^{(j)} & x_{t-w+2}^{(j)} & \dots & x_t^{(j)} \end{bmatrix} \in \mathbb{R}^{1 \times w}$ for $j \in \{1, 2, \dots, p\}$, and $X_t \in \mathbb{R}^{p \times w}$. In the following, elements belonging to the same component are coloured identically.

Furthermore, at time t , given a fixed auto-regressive order $d \in \{1, 2, \dots, w\}$, one may rearrange the finite set of observations in the current window X_t and construct each Hankel matrix [23, 5] $\mathcal{X}_t^{(j)} \in \mathbb{R}^{d \times (w-d+1)}$ from $X_t^{(j)}$, along with their concatenation $\mathcal{X}_t \in \mathbb{R}^{pd \times (w-d+1)}$ as

$$\forall j \in \{1, 2, \dots, p\}, \mathcal{X}_t^{(j)} := \begin{bmatrix} x_{t-w+1}^{(j)} & x_{t-w+2}^{(j)} & \dots & x_{t-d+1}^{(j)} \\ x_{t-w+2}^{(j)} & x_{t-w+3}^{(j)} & \dots & x_{t-d+2}^{(j)} \\ \vdots & \vdots & \ddots & \vdots \\ x_{t-w+d}^{(j)} & x_{t-w+d+1}^{(j)} & \dots & x_t^{(j)} \end{bmatrix} \Rightarrow \mathcal{X}_t := \begin{bmatrix} \mathcal{X}_t^{(1)} \\ \mathcal{X}_t^{(2)} \\ \vdots \\ \mathcal{X}_t^{(p)} \end{bmatrix}. \quad (2)$$

Formatting data within a Hankel matrix has been suggested by previous works in the dynamical systems [23, 5] and changepoint detection [28, 18] literature. The concatenated \mathcal{X}_t

is then used to learn the dynamical properties of the multivariate signal at time t within the current sliding window.

3.2 Learning and reconstructing the stream's dynamics

Our method leverages DMD to learn the dynamical properties of the input stream and flag times at which the underlying generating process of the dynamical system appears to have changed. Indeed, DMD provides a linear state-space model approximation of a nonlinear dynamical system by operating on delay-embedded data snapshots.

After computing $\mathcal{X}_t \in \mathbb{R}^{pd \times (w-d+1)}$ in Equation (2), we then perform DMD on \mathcal{X}_t by considering its $(w-d+1)$ columns as pd -dimensional snapshots. Incorporating time-delay embeddings is a typical technique in signal processing [28, 3] and allows one to express ergodic attractors of non-linear dynamical systems [37]. Performing DMD on time-delay embeddings rather than on the original observations is also known as Hankel DMD [5] or Higher-Order DMD [23]. In particular, we use this variant of DMD to be more flexible and account for signals with *low* spatial dependencies. Furthermore, DMD on time-delay embeddings has been shown to converge to the true eigenfunctions of the Koopman operator [5]. Hence, given a rank $r \leq \min\{pd, w-d+1\}$, we apply DMD on \mathcal{X}_t as described in Algorithm 2 and obtain spatial modes $\Phi_t \in \mathbb{C}^{pd \times r}$, dynamics $\Omega_t \in \mathbb{C}^{r \times r}$ and low-rank reconstruction of the Hankel batch $\hat{\mathcal{X}}_t \in \mathbb{R}^{pd \times (w-d+1)}$.

The DMD reconstruction of the Hankel batch $\hat{\mathcal{X}}_t$ produces multiple different estimates of the same original observations due to time-delay embeddings, as illustrated in Equation (3). Therefore, from the reconstructed delay-embedded snapshots $\hat{\mathcal{X}}_t$, one can recover many different reconstructions of the windowed batch X_t . For each component $j \in \{1, 2, \dots, p\}$, our reconstruction is defined as

$$\hat{\mathcal{X}}_t^{(j)} := \begin{bmatrix} \hat{x}_{t-w+1}^{(j),1} & \hat{x}_{t-w+2}^{(j),2} & \cdots & \hat{x}_{t-d+1}^{(j),w-d+1} \\ \hat{x}_{t-w+2}^{(j),1} & \hat{x}_{t-w+3}^{(j),2} & \cdots & \hat{x}_{t-d+2}^{(j),w-d+1} \\ \vdots & \vdots & \ddots & \vdots \\ \hat{x}_{t-w+d}^{(j),1} & \hat{x}_{t-w+d+1}^{(j),2} & \cdots & \hat{x}_t^{(j),w-d+1} \end{bmatrix} \Rightarrow \hat{X}_t^{(j)} := \begin{bmatrix} \hat{x}_{t-w+1}^{(j),1} \\ \hat{x}_{t-w+2}^{(j),2} \\ \vdots \\ \hat{x}_{t-d+1}^{(j),w-d+1} \\ \hat{x}_{t-d+2}^{(j),w-d+1} \\ \vdots \\ \hat{x}_t^{(j),w-d+1} \end{bmatrix}^\top, \quad (3)$$

i.e. by traversing the path of $\hat{\mathcal{X}}_t^{(j)} \in \mathbb{R}^{d \times (w-d+1)}$ first along its first row and then along the last column to obtain $\hat{X}_t^{(j)} \in \mathbb{R}^{1 \times w}$. Applying this block reconstruction to each component of the Hankel batch leads to a reconstruction of the original windowed batch again using concatenation

$$\hat{\mathcal{X}}_t := \begin{bmatrix} \hat{\mathcal{X}}_t^{(1)} \\ \hat{\mathcal{X}}_t^{(2)} \\ \vdots \\ \hat{\mathcal{X}}_t^{(p)} \end{bmatrix} \in \mathbb{R}^{pd \times (w-d+1)} \Rightarrow \hat{X}_t := \begin{bmatrix} \hat{X}_t^{(1)} \\ \hat{X}_t^{(2)} \\ \vdots \\ \hat{X}_t^{(p)} \end{bmatrix} \in \mathbb{R}^{p \times w}. \quad (4)$$

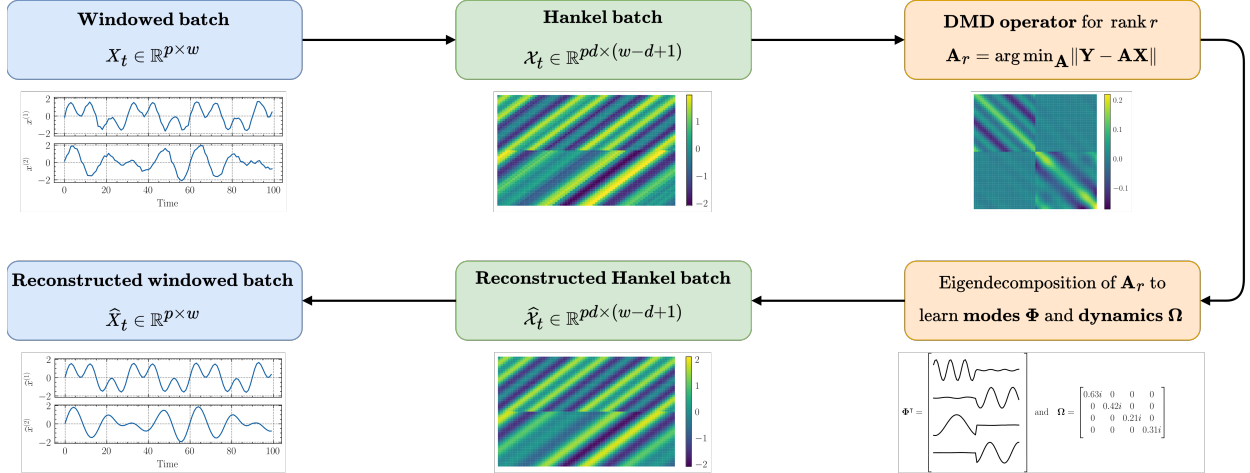


Figure 2: Illustration of the sequential data stream processing and reconstruction via DMD.

While this reconstruction is not unique, the one we consider in Equations (3) and (4) may be considered as *the most causal* since it only requires the first column of the windowed batch X_t , i.e. the true observation x_{t-w+1} , to compute the remaining $w - 1$ columns of the windowed batch $\hat{x}_{t-w+2}, \hat{x}_{t-w+3}, \dots, \hat{x}_t$ similarly to classical DMD settings. Our sequential transformation of the data and reconstruction of its dynamics is illustrated in Figure 2.

3.3 Detecting changepoints based on reconstruction error

After obtaining a low-rank reconstruction of the windowed batch \hat{X}_t , our method consists in detecting shifts in the data generating mechanism by monitoring the reconstruction quality [14]. Let ε_t denote the reconstruction error on the windowed batches, and let δ_t be the error increments at time t , where

$$\varepsilon_t := \frac{1}{pw} \|X_t - \hat{X}_t\|_F^2 \in \mathbb{R}^+, \quad \delta_t := \varepsilon_t - \varepsilon_{t-1} \in \mathbb{R}. \quad (5)$$

Distribution shifts in the data are expected to manifest as perturbations in the reconstruction error over time. While consecutive reconstruction error terms may be correlated due to their overlapping set of considered observations, their increments would be better modelled as stationary. Therefore, changepoints in the data can be detected by analysing the gradients of the reconstruction error. In discrete time settings with uniformly spaced observations, this approach is equivalent to monitoring the error increments, as defined in Equation (5). To detect changes in the gradient of the reconstruction error, we use an adaptive version of EWMA [33], detailed in Appendix 2. This distribution-free method has two hyperparameters, a learning rate $\lambda \in [0, 1]$ and a control limit $L \in \mathbb{R}_+^*$.

3.4 Algorithm summary

In summary, our proposal translates the task of changepoint detection in multivariate data, involving potentially different types of change, into the problem of univariate changepoint

Algorithm 1: $\hat{\tau} \leftarrow \text{SingleCP}(x_1, x_2, \dots, x_T \mid T_0, w, d, r, \lambda, L)$

```

/* Single changepoint detection via dynamic mode decomposition */
Input: Sequence of observations  $x_1, x_2, \dots, x_T \in \mathbb{R}^p$ 
Output: First detected changepoint in the sequence  $\hat{\tau}$ 
Parameters: Burn-in period  $T_0 \in \mathbb{N}$ , window length  $w \in \mathbb{N}$ , auto-regressive order  $d \leq w$ ,
                SVD rank  $r \leq \min\{pd, w - d + 1\}$ , adaptive EWMA learning rate  $\lambda \in [0, 1]$ 
                and limit  $L \in \mathbb{R}_+^*$ 
1 for  $t \in \{w, w + 1, \dots, T\}$  do
2    $X_t \leftarrow [x_{t-w+1}, x_{t-w+2}, \dots, x_t]$  /* Windowed batch (Equation (1)) */
3    $\mathcal{X}_t \leftarrow \text{Hankel}(X_t \mid d)$  /* Hankel batch (Equation (2)) */
4    $\{\hat{\mathcal{X}}_t, \Phi_t, \Omega_t\} \leftarrow \text{DMD}(\mathcal{X}_t \mid r)$  /* DMD on Hankel batch (Algorithm 2) */
5    $\hat{X}_t \leftarrow \text{Unroll}(\hat{\mathcal{X}}_t \mid d)$  /* Windowed batch reconstruction (Equations (3) and
      (4)) */
6    $\varepsilon_t \leftarrow \|X_t - \hat{X}_t\|_F^2$  /* Reconstruction error (Equation (5)) */
7    $\delta_t \leftarrow \varepsilon_t - \varepsilon_{t-1}$ 
8    $Z_t \leftarrow (1 - \lambda)Z_{t-1} + \lambda\delta_t$  /* Adaptive EWMA on increments (Definition A.2) */
9   if  $t > T_0$  and  $(Z_t > \mu_t + L\sigma_{Z_t}$  or  $Z_t < \mu_t - L\sigma_{Z_t})$  then
10    | return  $\hat{\tau} = t$  /* Detected changepoint */
11  end
12 end
13 return  $\hat{\tau} = \text{None}$  /* No detected changepoint */

```

detection in the reconstruction error, which is computed efficiently at each time step within sequential context windows. The reconstruction method is based on the DMD algorithm applied to time-delay embeddings of the original data, extracting accurate representations of the dynamics. Changes in the input stream may be detected as perturbations of the reconstruction error increments using an adaptive EWMA algorithm. This approach is summarised in Algorithm 1 for single changepoint detection.

3.5 Hyperparameter selection

Algorithm 1 requires specifying hyperparameters such as the window size w , the auto-regressive order d , and the rank r . To address the lack of prior knowledge for setting these parameters, we propose an approach that determines w , d , and r based on a burn-in period $T_0 \in \mathbb{N}$ in an unsupervised and data-driven manner.

Assuming a fixed burn-in period T_0 , we define a grid Θ satisfying the parameters constraints

$$\Theta := \{(w, d, r) \in \mathbb{N}^3 \mid w \leq T_0, d \leq w, r \leq \min\{pd, w - d + 1\}\},$$

where p is the dimension of the input stream. Running parallel competing models [20], hyperparameter selection is achieved by minimising the average reconstruction error, i.e.

$$\theta^* := \arg \min_{(w, d, r) \in \Theta} \frac{1}{T_0 - w + 1} \sum_{t=w}^{T_0-w+1} \varepsilon_t.$$

This approach is summarised in Algorithm 3 and discussed further in Appendix B.2. The remaining adaptive EWMA parameters λ and L are set by the user and control the overall sensitivity, although suggested empirical values from the EWMA literature [25] are $\lambda \in [0.05, 1]$ and $L \in [2.4, 3]$.

3.6 Theoretical analysis

Theorem 3.1. Consider a p -dimensional stream of observations monitored via Algorithm 1. Let $\mathbf{A} \in \mathbb{C}^{pd \times pd}$ be the DMD operator at time t and let $\tilde{\mathbf{A}} \in \mathbb{C}^{pd \times pd}$ denote the DMD operator at time $t + 1$. Then, there exists a perturbation matrix $\mathbf{E} \in \mathbb{C}^{pd \times pd}$ such that $\tilde{\mathbf{A}} = \mathbf{A} + \mathbf{E}$, where the closed-form of \mathbf{E} is detailed in Appendix C.1. Furthermore, assuming that the DMD operator \mathbf{A} is diagonalisable, then the following results hold:

- (i) Eigenvalues (dynamics): let $\tilde{\lambda} \in \sigma(\tilde{\mathbf{A}})$, i.e. $\tilde{\lambda}$ is an eigenvalue of $\tilde{\mathbf{A}}$, then

$$\min_{\lambda \in \sigma(\mathbf{A})} |\tilde{\lambda} - \lambda| \leq \kappa_2(\Phi) \|\mathbf{E}\|_2,$$

where $\|\mathbf{E}\|_2$ denotes the matrix 2-norm of \mathbf{E} , $\kappa_2(\Phi) = \|\Phi\|_2 \|\Phi^{-1}\|_2$ is the condition number of $\Phi \in \mathbb{C}^{pd \times pd}$ and Φ is the eigenvectors matrix of \mathbf{A} .

- (ii) Eigenvectors (modes): let $\tilde{\phi}_k \in \mathbb{C}^{pd}$ and $\phi_k \in \mathbb{C}^{pd}$ denote normalised eigenvectors of $\tilde{\mathbf{A}}$ and \mathbf{A} respectively for $k \in \{1, 2, \dots, pd\}$, then

$$\|\tilde{\phi}_k - \phi_k\|_2 \leq \frac{\|\mathbf{E}\|_2}{\min_{j \neq k} |\lambda_k - \lambda_j|} + \mathcal{O}(\|\mathbf{E}\|_2^2), \forall k \in \{1, 2, \dots, pd\}.$$

Consequences. Theorem 3.1 shows that, following our approach, within consecutive time steps in which we model the modes and dynamics of the input stream as pairs of eigenvalues and eigenvectors of the DMD operator, the recently estimated modes and dynamics are *close* to the previous ones provided that the perturbation due to the sliding window and the new observed datum is *small*. Indeed, the closed-form of \mathbf{E} in Appendix C.1 shows that the perturbation is proportional to the predictive error of the previous DMD model on the new snapshot. However, if the underlying generating process has not changed, the predictive accuracy remains *high*, provided that parameters are set to minimise the error as discussed in Section 3.5. Therefore, when monitoring a sequence with no change in the underlying generating process, modes and dynamics extracted by the sequential DMD models are similar, leading to a *stable* reconstruction error.

3.7 Computational complexity

Theorem 3.2. The computational complexity of Algorithm 1 in the context of single changepoint detection is $\mathcal{O}(pd(w - d) \cdot \min\{pd, w - d\})$, where p is the dimension of the input stream, w is the window length and d denotes the auto-regressive order.

Theorem 3.2 shows that complexity scales linearly with the dimension, in addition to that our proposed approach is efficient and its complexity is simply determined by its parameters.

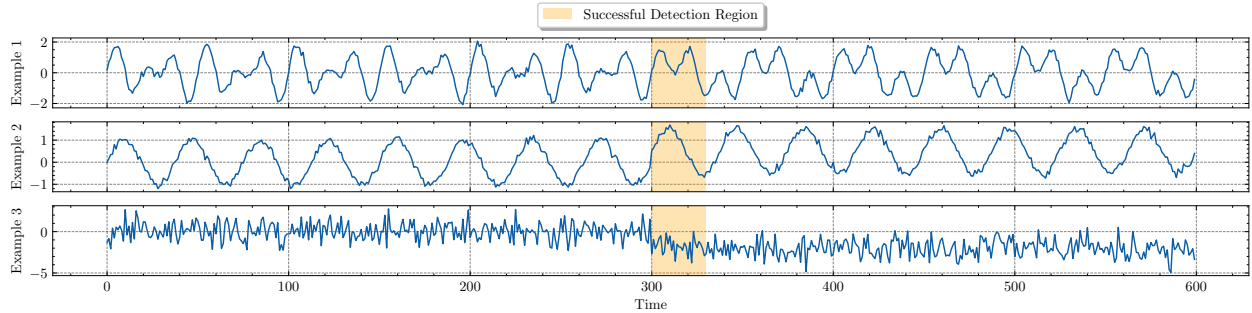


Figure 3: Three examples of sequences considered in synthetic data simulations.

Figure 5 in Appendix C.2 illustrates how the complexity of our proposed method for single changepoint detection scales with varying dimension, window length and auto-regressive order. Further discussion on complexity can be found in Appendix C.2, particularly Corollary C.7 on hyperparameter selection.

4 Experiments and simulations

Algorithm 4 in Appendix B.3 describes our proposed method with auto-adaptive parameters combining Algorithms 1 and 3 to process data streams with multiple changepoints. We conduct a comparative evaluation of the CPDMD algorithm against six established changepoint detection methods: EWMA [33], EWMVar [26], RuLSIF [52], BOCPDMS [20], mSSA and its variant mSSA-MW [3]. A comparison of these selected algorithms capabilities can be found in Table 4 in Appendix D.2.2. We do not compare to [43, 17] cited in Section 2.1.1; those works focused on developing DMD methodology in which changepoint detection was only considered as a secondary application, without a comprehensive performance assessment, and implementations of these methods are unavailable.

The simulation study presented in Section 4.1 focuses on online changepoint detection in synthetic univariate time series that may exhibit trend and seasonality, with a single change in the data generating mechanism. We focus our simulation study on the single changepoint setting, which is a common approach [34, 10], as poor performance in this simpler case is indicative of potential struggles with the more challenging multiple changepoint scenario, and the latter may be addressed, among other approaches, by iteratively restarting a performing single changepoint detector. We reserve comprehensive multivariate simulations for future work in the interest of conciseness, since changepoint detection of multivariate data is more complex with a wider variety of change types. However, since the problem of multiple changepoint detection in multivariate data remains important across various application domains, we demonstrate the effectiveness of CPDMD on real-world datasets in Section 4.2.

4.1 Synthetic data

Types of change. We evaluate algorithms performance on seasonal univariate streams containing a specific type of change: periodicity, location, amplitude, trend, and double periodicity. We also consider streams that do not present any seasonality, with changes in

the mean or variance. See Figure 3 for examples of these sequence types and Appendix D.2.1 for additional details.

Simulation settings. Each algorithm requires parameters to be set. To reduce any bias induced by parameters specification, we follow the recommendations from [49] by reporting the performance obtained with default parameters, along with the best performance from a grid of parameters which is defined for each selected algorithm in Appendix D.2.2.

Performance metrics. We assess performance via well-established online changepoint detection performance metrics: precision P , recall R , F_1 -Score and Average Run Lengths ARL_0 and ARL_1 . We provide definitions of these metrics in Appendix 2. The standard errors for P , R , and F_1 , computed via a bootstrap procedure, and $SDRL_0$ and $SDRL_1$ are shown in parentheses. An effective algorithm would aim to maximise the F_1 -Score and ARL_0 , while minimising ARL_1 .

Results. Table 1 shows that CPDMD significantly outperforms every other considered method in terms of precision, recall and F_1 -Score for both best and default parameters, while the corresponding values of ARL_0 and ARL_1 are often ranked among the two best ones. However, since no other method achieves similar F_1 -Scores, the interpretation is more complex and strictly comparing raw values would make the comparison of ARLs biased. This is indeed well shown and complemented by Figure 4 which provides a better overview of the performance of each algorithm across all tested sets of parameters. CPDMD reaches the highest values of F_1 -Score for the lowest values of ARL_1 . Moreover, given a desired sensitivity defined by a desired ARL_0 , simulations show that there always exists a CPDMD model which obtains the best F_1 -Score. Another important aspect of changepoint detection algorithms is the scaling law between ARL_0 and ARL_1 , and our proposed approach shows among the best scaling laws, i.e. given any desired value of ARL_0 , it has among the lowest ARL_1 . CPDMD is also shown to be robust to parameters selection, with close performance of default and best parameters, along with no widely scattered points in Figure 4. Our proposed approach performance is followed by EWMA and RuLSIF, while the latter was originally proposed in retrospective changepoint detection and could be adapted to sequential context using an *a priori unknown* threshold as the decision rule. Note that due to its increased computational complexity on long sequences, the ARL_0 of BOCPDMS is not estimated: however, precision, recall, F_1 -Score and ARL_1 of the BOCPDMS algorithm on synthetic data is detailed in Appendix D.2.3. Results per change type are provided in Appendix D.2.

4.2 Real-world data

Datasets. We consider three real-world datasets from various application domains. The HASC dataset [16] is an activity recognition dataset, consisting of three-dimensional acceleration measurements from wearable devices, in which the goal is to detect when a user switches from an activity to another. The Digits dataset consists of sequences of 8×8 greyscale images extracted from [51], where images of the same digit are displayed for a specific duration before switching to a different digit. The Yahoo Webscope S5 dataset [22] is a collection of

Table 1: Evaluation of selected changepoint detection algorithms on synthetic data, comparing performance achieved with the parameter set yielding highest F_1 -Score (*best*) against default parametrisation (*default*). We highlight the top two performance metrics for each set of parameters in bold.

Algorithm	Params.	P	R	F_1	ARL_1	ARL_0
EWMA	Best	.669 (.004)	.474 (.003)	.555 (.003)	9.78 (7.44)	71085.25 (41976.94)
	Default	.188 (.003)	.181 (.003)	.185 (.003)	5.88 (5.11)	4261.15 (18156.77)
EWMVar	Best	.275 (.005)	.131 (.002)	.178 (.003)	10.96 (6.86)	71202.77 (45092.24)
	Default	.452 (.009)	.089 (.002)	.148 (.003)	12.36 (7.40)	99900.00 (0.00)
RuLSIF	Best	.537 (.013)	.414 (.010)	.468 (.011)	19.01 (6.80)	41934.74 (49177.96)
	Default	.448 (.011)	.364 (.010)	.401 (.010)	23.58 (4.61)	57147.14 (49746.53)
mSSA	Best	.475 (.005)	.266 (.003)	.341 (.004)	6.91 (6.09)	43786.39 (47153.54)
	Default	.304 (.003)	.210 (.002)	.248 (.003)	6.28 (5.80)	27023.57 (42587.84)
mSSA-MW	Best	.443 (.005)	.313 (.004)	.367 (.004)	8.79 (5.87)	13834.54 (32965.67)
	Default	.043 (.001)	.041 (.001)	.042 (.001)	9.11 (7.29)	8210.28 (20999.07)
CPDMD	Best	.960 (.001)	.902 (.002)	.930 (.002)	7.11 (6.14)	4034.30 (3997.10)
	Default	.978 (.001)	.807 (.003)	.884 (.002)	9.53 (6.47)	58341.28 (38161.07)

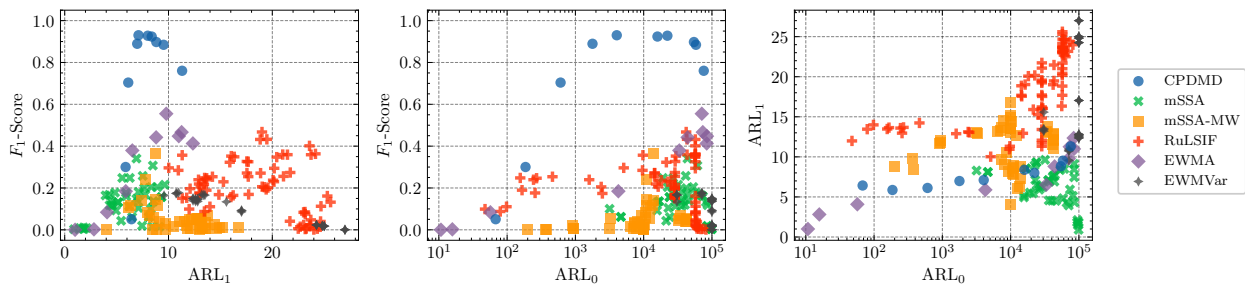


Figure 4: Performance comparison of changepoint detection algorithms on synthetic data across all scenarios. Each dot corresponds to an algorithm with a specific choice of parameter values.

univariate time series extracted from real-world web traffic. We provide additional description of these datasets in Appendix D.3.1.

Simulation settings. Similarly to simulations on synthetic data, we evaluate the performance of each selected algorithm on a grid of parameters with consistency across burn-in periods of each algorithm and dataset. This grid is detailed in Appendix D.3.2. Note that both EWMA and EWMVar are univariate methods, and there may exist many different ways to use those on multivariate streams. In this work, we adapt them to the multivariate datasets by running separate instances per component and taking the union of detected changepoints across all components.

Performance metrics. We assess the empirical performance of each algorithm via F_1 -Score and covering metric \mathcal{C} , both defined in Appendix 2. Since changepoint locations in real-world data are the result of human annotations, shifts may be detected slightly before their location times, making the computation of ARL_1 intractable. Instead, we use the covering metric,

Table 2: Evaluation of selected changepoint detection algorithms on real-world data, comparing performance achieved with the parameter set yielding highest F_1 -Score (*best*) against default parametrisation (*default*). We highlight the top two performance metrics for each set of parameters in bold.

Algorithm	Params.	HASC		Digits				Yahoo	
		F_1	\mathcal{C}	F_1	\mathcal{C}	F_1	\mathcal{C}	F_1	\mathcal{C}
EWMA	Best	.347 (.086)	.470 (.081)	.067 (.005)	.329 (.044)	.454 (.300)	.593 (.237)		
	Default	.216 (.030)	.400 (.072)	.025 (.001)	.129 (.017)	.240 (.248)	.428 (.183)		
EWMVar	Best	.460 (.069)	.638 (.077)	.091 (.006)	.262 (.029)	.442 (.365)	.700 (.240)		
	Default	.384 (.039)	.615 (.059)	.053 (.004)	.183 (.018)	.380 (.358)	.642 (.255)		
BOCPDMS	Best	.209 (.121)	.466 (.096)	.037 (.001)	.036 (.002)	.096 (.217)	.616 (.273)		
	Default	.194 (.114)	.456 (.089)	.013 (.002)	.032 (.004)	.080 (.195)	.610 (.273)		
RuLSIF	Best	.420 (.080)	.512 (.055)	N/A (N/A)	N/A (N/A)	.247 (.352)	.573 (.221)		
	Default	.267 (.095)	.563 (.073)	N/A (N/A)	N/A (N/A)	.232 (.361)	.614 (.234)		
mSSA	Best	.213 (.169)	.260 (.145)	.073 (.162)	.265 (.096)	.540 (.325)	.710 (.212)		
	Default	.183 (.126)	.239 (.137)	.073 (.162)	.267 (.090)	.540 (.325)	.710 (.212)		
mSSA-MW	Best	.486 (.096)	.586 (.046)	.206 (.200)	.555 (.121)	.403 (.298)	.578 (.211)		
	Default	.403 (.086)	.557 (.063)	.145 (.130)	.592 (.106)	.399 (.296)	.548 (.224)		
CPDMD	Best	.499 (.077)	.608 (.065)	.645 (.274)	.657 (.148)	.526 (.332)	.726 (.199)		
	Default	.476 (.109)	.539 (.092)	.483 (.296)	.484 (.200)	.526 (.332)	.726 (.199)		

often used in offline changepoint detection as a good measure of the quality of a segmentation with multiple changepoints.

Results. Table 2 demonstrates superior overall performance of CPDMD compared to other methods. CPDMD consistently ranks among the top two methods across the two considered metrics. Similar to the synthetic data simulations, this experiment suggests that CPDMD is robust to parameter selection, achieving near-optimal F_1 -Scores with default parameters, particularly on the HASC and Yahoo datasets. On the Digits dataset, CPDMD outperforms all other algorithms, indicating its suitability for high-dimensional datasets. While some methods, such as mSSA-MW on the HASC dataset and mSSA on the Yahoo dataset, show comparable performance, no single method matches CPDMD’s overall effectiveness. RuLSIF’s performance cannot be computed for the Digits dataset due to matrix inversion issues, likely due to high dimensionality and low variability of certain pixels. Overall, the performance gap between CPDMD and other methods is smaller on real-world data compared to synthetic data. This may be due to CPDMD’s sensitivity to subtle changes, which might not be labelled as changepoints in the datasets, increasing false positives. Additionally, annotation fluctuations, especially in the HASC dataset, might cause delays in labelling actual changes. Lastly, results on the Yahoo dataset demonstrate CPDMD’s efficiency for both change and anomaly detection.

5 Conclusion

In this paper we propose CPDMD, a nonparametric data-driven approach that leverages DMD to detect changepoints in multivariate streaming data for a variety of change types. This method has excellent performance on both synthetic and real-world datasets.

Limitations. Since CPDMD detects a change in reconstruction error, it is unclear what type of change actually occurs; monitoring the modes and dynamics directly could provide insight into the type of change. The hyperparameter selection approach is based on a grid search, which is performant but could potentially be improved. One potential improvement could be to replace the adaptive EWMA with a method better suited to detect changes in the reconstruction error, although we did not find a better method from empirical results. These research areas are left for future work.

6 Acknowledgements

Victor Khamesi is funded by a Roth Scholarship from the Department of Mathematics, Imperial College London. Ed Cohen acknowledges funding from the EPSRC, grant number EP/X002195/1.

A Background

Definition A.1 (EWMA algorithm [33]). Consider a univariate stream y_1, y_2, \dots with mean μ and variance σ^2 . Let $\lambda \in [0, 1]$ denote the learning rate and $L \in \mathbb{R}_+^*$ a control parameter for the algorithm's sensitivity. Let $Z_0 = \mu$ and, for $t \in \mathbb{N}^*$

$$Z_t := (1 - \lambda)Z_{t-1} + \lambda y_t.$$

Then, the standard deviation of Z_t is

$$\sigma_{Z_t} = \sigma \sqrt{\frac{\lambda}{2 - \lambda} (1 - (1 - \lambda)^{2t})},$$

and a change is detected when either $Z_t > \mu + L\sigma_{Z_t}$ or $Z_t < \mu - L\sigma_{Z_t}$.

We introduce in Definition A.2 a slightly modified version of the original EWMA algorithm introduced by [33] where the mean and variance of the input stream are sequentially updated rather than being set to estimates on historical data.

Definition A.2 (Adaptive EWMA algorithm). Consider a univariate stream y_1, y_2, \dots with both unknown mean μ and variance σ^2 . Let $\lambda \in [0, 1]$ denote the learning rate and $L \in \mathbb{R}_+^*$ a control parameter for the algorithm's sensitivity. Let $Z_1 = y_1$ and, for $t \geq 2$,

$$Z_t := (1 - \lambda)Z_{t-1} + \lambda y_t.$$

Let μ_t and σ_t^2 denote sequential estimates of the input mean and variance respectively computed as in Lemma C.5. The standard deviation of Z_t is computed as

$$\sigma_{Z_t} = \sigma_t \sqrt{\frac{\lambda}{2 - \lambda} (1 - (1 - \lambda)^{2t})},$$

and a change is detected when either $Z_t > \mu_t + L\sigma_{Z_t}$ or $Z_t < \mu_t - L\sigma_{Z_t}$.

Definition A.3 (Average run lengths [29]). Consider a stream with a changepoint located at time τ , and assume the stream is monitored by an online changepoint detection algorithm which infers the first changepoint of the sequence, denoted as $\hat{\tau}$. Then, the Average Run Length 0 (ARL₀) is computed as the average number of observations until a changepoint is detected, when the algorithm is run over a sequence with no changepoint, i.e.

$$\text{ARL}_0 := \mathbb{E}[\hat{\tau} \mid \tau \rightarrow \infty].$$

The Average Run Length 1 (ARL₁) is computed as the average number of observations between a changepoint location and it is being detected, i.e.

$$\text{ARL}_1 := \mathbb{E}[\hat{\tau} - \tau \mid \hat{\tau} \geq \tau].$$

Hence, an effective algorithm should aim to maximise the ARL₀ while minimising the ARL₁.

In practice, for a given algorithm, we estimate the ARL_1 by running simulations on multiple data streams with a changepoint and obtaining for each sequence the detection delay, conditioning on correct detections and therefore excluding false detections from the computation. Thus, the ARL_1 is computed by averaging these delay values, and the corresponding standard deviation $SDRL_1$ (standard deviation run length) is obtained by taking the sample standard deviation of these run lengths. Similarly, we estimate the ARL_0 by running a given algorithm on multiple *sufficiently long* sequences without changepoints and obtain the corresponding run lengths as the first time to false detection. Then, the ARL_0 is computed by averaging these run lengths and its corresponding $SDRL_0$ by estimating the standard deviation of the run lengths. In practice, we may need to truncate the time series length for some algorithms with parameters leading to low sensitivity (see Table 3).

Definition A.4 (Precision, recall, and F_1 -Score [19, 49]). Consider a sequence with n changepoints denoted as $\tau_1, \tau_2, \dots, \tau_n$ and m detected changepoints $\hat{\tau}_1, \hat{\tau}_2, \dots, \hat{\tau}_m$. The set of correctly detected changepoints, or set of true positives, is defined as

$$\mathcal{TP} := \{\tau_i \mid \exists \hat{\tau}_j : \mu_l \leq \hat{\tau}_j - \tau_i \leq \mu_r\},$$

where $\mu_l \geq 0$ is a left margin and $\mu_r \geq 0$ is a right margin, defining the detection acceptance region around the true changepoint.

As in classical binary classification settings, the performance of a changepoint detection algorithm may be expressed in terms of precision P , defined as the ratio of correctly detected changepoints over the number of detected changepoints, and recall R , defined as the ratio of correctly detected changepoints over the number of true changepoints, i.e.

$$P := \frac{\text{card}(\mathcal{TP})}{m} \text{ and } R := \frac{\text{card}(\mathcal{TP})}{n}.$$

The corresponding F_1 -Score is defined as

$$F_1 := \frac{2PR}{P + R}$$

Remark A.5. The left margin accomodates the detection of a changepoint preceeding the closest true annotated changepoint, particularly to account for fluctuating annotations decisions in real-world data. The right margin extends the acceptance region on the right, defining the acceptable range within which a detected change can be reasonably associated with the most recent true change.

Definition A.6 (Covering [6, 49]). Consider a sequence of length T with true changepoints defined by the ordered set $\mathcal{T} = \{\tau_1, \tau_2, \dots, \tau_n\}$ with $\tau_i \in [1, T]$ for $i \in \{1, 2, \dots, n\}$ and $\tau_i < \tau_j$ for $i < j$. Then, \mathcal{T} implies a partition \mathcal{G} of the interval $[1, T]$ into disjoint sets \mathcal{A}_j , where \mathcal{A}_j is the segment from τ_{j-1} to $\tau_j - 1$, for $j \in \{1, 2, \dots, n + 1\}$, with convention $\tau_0 = 1$ and $\tau_{n+1} = T + 1$.

For two sets $\mathcal{A}, \mathcal{A}' \subseteq [1, T]$, the Jaccard index also known as Intersection over Union, is given by

$$J(\mathcal{A}, \mathcal{A}') := \frac{\text{card}(\mathcal{A} \cap \mathcal{A}')}{\text{card}(\mathcal{A} \cup \mathcal{A}')}$$

For a sequence of length T , given a ground truth partition \mathcal{G} and a predicted partition \mathcal{G}' , the covering metric is defined as

$$\mathcal{C}(\mathcal{G}, \mathcal{G}') := \frac{1}{T} \sum_{\mathcal{A} \in \mathcal{G}} \text{card}(\mathcal{A}) \cdot \max_{\mathcal{A}' \in \mathcal{G}'} J(\mathcal{A}, \mathcal{A}').$$

We rely on coding implementations of F_1 -Score and covering provided by the Alan Turing Institute GitHub repository <https://github.com/alan-turing-institute/TCPDBench> and detailed in [49].

B Algorithms pseudo-code

B.1 Dynamic mode decomposition

We provide in Algorithm 2 a pseudo-code for the dynamic mode decomposition algorithm as introduced by [36] based on singular value decomposition.

Algorithm 2: $\{\hat{\mathbf{x}}, \Phi, \Omega\} \leftarrow \text{DMD}(\mathbf{x} \mid r)$

```

/* Dynamic Mode Decomposition */
Input: Snapshots  $\mathbf{x} = [\mathbf{x}_1, \mathbf{x}_2, \dots, \mathbf{x}_m] \in \mathbb{R}^{p \times m}$ 
Output: Low-rank reconstruction  $\hat{\mathbf{x}} \in \mathbb{R}^{p \times m}$ , modes  $\Phi \in \mathbb{C}^{p \times r}$ , dynamics  $\Omega \in \mathbb{C}^{r \times r}$ 
Parameters: SVD rank  $r \leq \min(p, m)$ 
1 /* Lagged matrices (Equation (6)) */
2  $\mathbf{X} \leftarrow [\mathbf{x}_1, \mathbf{x}_2, \dots, \mathbf{x}_{m-1}]$ 
3  $\mathbf{Y} \leftarrow [\mathbf{x}_2, \mathbf{x}_3, \dots, \mathbf{x}_m]$ 
4 /* Singular Value Decomposition */
5  $\mathbf{U}, \Sigma, \mathbf{V} \leftarrow \text{SVD}(\mathbf{X})$  where  $\mathbf{X} \simeq \mathbf{U}\Sigma\mathbf{V}^*$ ,  $\mathbf{U} \in \mathbb{C}^{p \times r}$ ,  $\Sigma \in \mathbb{C}^{r \times r}$  and  $\mathbf{V} \in \mathbb{C}^{(m-1) \times r}$ 
6 /* Operator projected onto principal modes */
7  $\tilde{\mathbf{A}}_r \leftarrow \mathbf{U}^* \mathbf{Y} \mathbf{V} \Sigma^{-1}$ 
8 /* Eigendecomposition */
9  $\Lambda, \mathbf{W} \leftarrow \text{eig}(\tilde{\mathbf{A}}_r)$  where  $\tilde{\mathbf{A}}_r \mathbf{W} = \mathbf{W} \Lambda$ ,  $\mathbf{W} \in \mathbb{C}^{r \times r}$  and  $\Lambda = \text{diag}(\lambda_1, \lambda_2, \dots, \lambda_r) \in \mathbb{C}^{r \times r}$ 
10 /* Dynamics, modes and amplitudes */
11  $\Omega \leftarrow \text{diag}(\omega_1, \omega_2, \dots, \omega_r)$  where  $\omega_j = \log(\lambda_j) / \Delta t$  for  $j \in \{1, 2, \dots, r\}$ 
12  $\Phi \leftarrow \mathbf{Y} \mathbf{V} \Sigma^{-1} \mathbf{W}$ 
13  $\mathbf{b} \leftarrow \Phi^\dagger \mathbf{x}_1$ 
14 /* Reconstruction */
15 for  $k \in \{1, 2, \dots, m\}$  do
16 |  $\hat{\mathbf{x}}_k \leftarrow \Phi \exp(\Omega(k-1)\Delta t) \mathbf{b}$ 
17 end
18  $\hat{\mathbf{x}} \leftarrow [\hat{\mathbf{x}}_1, \hat{\mathbf{x}}_2, \dots, \hat{\mathbf{x}}_m]$ 
19 return  $\{\hat{\mathbf{x}}, \Phi, \Omega\}$ 

```

Dynamic mode decomposition algorithm. Assume one monitors a dynamical system and collects m observations $\mathbf{x}_1, \mathbf{x}_2, \dots, \mathbf{x}_m \in \mathbb{R}^p$. Observations are compiled in two distinct lagged data sets $\mathbf{X}, \mathbf{Y} \in \mathbb{R}^{p \times (m-1)}$

$$\mathbf{X} = \begin{bmatrix} \mathbf{x}_1 & \mathbf{x}_2 & \cdots & \mathbf{x}_{m-1} \end{bmatrix}, \quad \mathbf{Y} = \begin{bmatrix} \mathbf{x}_2 & \mathbf{x}_3 & \cdots & \mathbf{x}_m \end{bmatrix}. \quad (6)$$

Then, DMD consists in finding the *best-fit* linear operator $\mathbf{A} \in \mathbb{R}^{p \times p}$ such that $\mathbf{Y} = \mathbf{A}\mathbf{X}$. In fact, the optimal solution is defined as $\tilde{\mathbf{A}} = \mathbf{Y}\mathbf{X}^\dagger$ where \mathbf{X}^\dagger denotes the Moore-Penrose pseudo-inverse of \mathbf{X} . This regression problem may be solved using classical least-squares optimisation. However, DMD rather estimates a low-rank eigendecomposition of the linear operator $\tilde{\mathbf{A}}$, since the complete estimation of $\tilde{\mathbf{A}} \in \mathbb{R}^{p \times p}$ may become intractable for values of $p \gg 1$ [36]. Hence, DMD solves the following optimisation problem

$$\tilde{\mathbf{A}}_r = \arg \min_{\mathbf{A} \in \mathbb{R}^{p \times p}} \|\mathbf{Y} - \mathbf{A}\mathbf{X}\|_F^2 \text{ with } \text{rank } \mathbf{A} \leq r,$$

using singular value decomposition, which results in extracting and learning dynamics $\mathbf{\Omega} \in \mathbb{C}^{r \times r}$ and spatial modes $\mathbf{\Phi} \in \mathbb{C}^{p \times r}$ directly from the eigendecomposition of the best-fit operator $\tilde{\mathbf{A}}_r$. A low-rank reconstruction of the input is computed as

$$\hat{\mathbf{x}}_{t+1} = \mathbf{\Phi} \exp(\mathbf{\Omega}t) \mathbf{\Phi}^\dagger \mathbf{x}_1, \text{ for } t \in \{0, 1, \dots, m-1\}.$$

The DMD algorithm is described in Algorithm 2. Note that DMD extracts pairs of modes and their associated dynamics: modes can be interpreted as coherent structures or spatial *shapes* of the signal, and dynamics encode the temporal evolution of the related mode, with real part corresponding to their growth and imaginary part to their oscillating frequency. Computational complexity of DMD algorithm is described in Lemma C.6 in Appendix C.2.

B.2 Unsupervised hyperparameter selection

We provide in Algorithm 3 a pseudo-code for our proposed hyperparameter selection on burn-in period.

Algorithm 3: $\theta^* = (w, d, r) \leftarrow \text{HyperparameterSelection}(x_1, x_2, \dots, x_{T_0} \mid T_0)$

```

/* Hyperparameter selection by average reconstruction error minimisation */
Input: Sequence of observations on burn-in period  $x_1, x_2, \dots, x_{T_0} \in \mathbb{R}^p$ 
Output: Optimal parameters  $\theta^* = (w, d, r)$ 
Parameters: Burn-in period  $T_0 \in \mathbb{N}$ 
1 /* Grid of parameters generation and initalisation */
2  $\Theta \leftarrow \text{grid}(T_0, p)$ 
3  $\varepsilon^* \leftarrow \infty$ 
4 /* Explore possible models (in parallel) */
5 for  $(w, d, r) \in \Theta$  do
6    $\varepsilon_t \leftarrow 0$  for  $t \in \{w, w + 1, \dots, T_0\}$ 
7   for  $t \in \{w, w + 1, \dots, T_0\}$  do
8     /* Sequential DMD on Hankel batches and reconstruction */
9      $X_t \leftarrow [x_{t-w+1}, x_{t-w+2}, \dots, x_t]$ 
10     $\mathcal{X}_t \leftarrow \text{Hankel}(X_t \mid d)$ 
11     $\{\hat{\mathcal{X}}_t, \Phi_t, \Omega_t\} \leftarrow \text{DMD}(\mathcal{X}_t \mid r)$ 
12     $\hat{X}_t \leftarrow \text{Unroll}(\hat{\mathcal{X}}_t \mid d)$ 
13    /* Reconstruction error */
14     $\varepsilon_t \leftarrow \|X_t - \hat{X}_t\|_F^2$ 
15  end
16  /* Average reconstruction error */
17   $\varepsilon \leftarrow \frac{1}{T_0 - w + 1} \sum_{t=w}^{T_0} \varepsilon_t$ 
18  if  $\varepsilon < \varepsilon^*$  then
19    /* Update best parameters and error */
20     $\varepsilon^* \leftarrow \varepsilon$ 
21     $\theta^* \leftarrow (w, d, r)$ 
22  end
23 end
24 return  $\theta^* = (w, d, r)$ 

```

Classical hyperparameter selection methods. On the one hand, classical unsupervised selection techniques involve the definition of a criterion to optimise, such as AIC [2] or BIC [38]. Such criteria are often parametric: they compute a likelihood function and thus require distribution assumptions. On the other hand, some hyperparameter selection methods rely on heuristics, such as the elbow [44] or silhouette [35] methods in clustering, but are not strict objective functions to optimise. Moreover, in contrast to iterative and sequential approaches such as Bayesian optimisation, our hyperparameter selection necessitates a streaming paradigm, where operations may be executed concurrently on different threads as suggested in [20], to enable real-time processing.

Approximation vs. reconstruction. Note that this hyperparameter selection procedure does not simply choose the most complex model on the grid of tested parameters: while at fixed window length w and auto-regressive order d , the approximation error of DMD would decrease when increasing the rank of the decomposition r , it may not be the case for the average reconstruction error. This is the result of DMD reconstruction being based on learned modes and dynamics rather than simply multiplying the first lagged matrix by the DMD operator. Indeed, the approximation error may be seen as a one-step ahead forecasting optimisation, where each observed snapshot is used to forecast the next one. In the contrary, the reconstruction error could be considered as a multiple steps ahead forecasting, where only the first snapshot is used to recurrently predict the next ones from the learned modes and dynamics. The optimal window length w , the auto-regressive order d and the rank r are typically determined by the underlying dynamical system properties.

Practical implementation. In practice, not all triplets of Θ can be explored and truncation of the parameters space is necessary due to computational constraints (e.g., the number of threads). We further discuss the grid generation process used in simulations and experiments in Appendix D.

B.3 Multiple changepoints detection

We provide in Algorithm 4 a pseudo-code for our proposed method in the context of multiple changepoints, with parameters being auto-adjusted to the post-change distribution after each detected changepoint.

Algorithm 4: $\hat{\tau} \leftarrow \text{CPDMD}(x_1, x_2, \dots, x_T \mid T_0, \lambda, L)$

```

/* Multiple changepoint detection via DMD with hyperparameter selection */
Input: Sequence of observations  $x_1, x_2, \dots, x_T \in \mathbb{R}^p$ 
Output: List of detected changepoints in the sequence  $\hat{\tau}$ 
Parameters: Burn-in period  $T_0 \in \mathbb{N}$ , adaptive EWMA learning rate  $\lambda \in [0, 1]$  and limit
                 $L \in \mathbb{R}_+^*$ 
1  $\hat{\tau} \leftarrow 1$ 
2  $\hat{\tau} \leftarrow \emptyset$ 
3 while  $\hat{\tau} \neq \text{None}$  do
4     /* Check that there are enough remaining samples */
5     if  $T - \hat{\tau} \geq T_0$  then
6         /* Hyperparameter selection on new data distribution (Algorithm 3) */
7          $\theta^* = (w, d, r) \leftarrow \text{HyperparameterSelection}(x_\tau, x_{\tau+1}, \dots, x_{T_0} \mid T_0)$ 
8         /* Find the next changepoint in the remaining sequence (Algorithm 1) */
9          $\hat{\tau} \leftarrow \text{SingleCP}(x_\tau, x_{\tau+1}, \dots, x_T \mid T_0, w, d, r, \lambda, L)$ 
10    else
11         $\hat{\tau} \leftarrow \text{None}$ 
12    end
13    /* Add the new detected changepoint */
14     $\hat{\tau} \leftarrow \hat{\tau} \cup \{\hat{\tau}\}$ 
15 end
16 return  $\hat{\tau}$ 

```

C Theoretical analysis

C.1 Spectral properties of the DMD operator

C.1.1 Windowed incremental algorithms

Lemma C.1 (Windowed incremental SVD algorithm, Proposition 2 from [4]). Consider a windowed dataset

$$\mathbf{X}_k = \begin{bmatrix} \mathbf{x}_{k-w+1} & \mathbf{x}_{k-w+2} & \cdots & \mathbf{x}_k \end{bmatrix} \in \mathbb{R}^{n \times w},$$

where n is the dimension of the measurements and w is the window length. Consider the other windowed dataset corresponding to the consecutive window

$$\mathbf{X}_{k+1} = \begin{bmatrix} \mathbf{x}_{k-w+2} & \mathbf{x}_{k-w+3} & \cdots & \mathbf{x}_{k+1} \end{bmatrix} \in \mathbb{R}^{n \times w}.$$

Assume the SVD of \mathbf{X}_k is known: $\mathbf{X}_k = \mathbf{U}_{\mathbf{X}_k} \Sigma_{\mathbf{X}_k} \mathbf{V}_{\mathbf{X}_k}^*$. Then, the SVD of \mathbf{X}_{k+1} can be computed from the SVD of \mathbf{X}_k as follows.

Define the new dataset $\hat{\mathbf{X}}_k$ such that the first column of \mathbf{X}_k is eliminated

$$\hat{\mathbf{X}}_k = \begin{bmatrix} \mathbf{x}_{k-w+2} & \mathbf{x}_{k-w+3} & \cdots & \mathbf{x}_k \end{bmatrix} \in \mathbb{R}^{n \times (w-1)}.$$

Then, the SVD of $\hat{\mathbf{X}}_k$ is given by $\hat{\mathbf{X}}_k = \mathbf{U}_{\hat{\mathbf{X}}_k} \Sigma_{\hat{\mathbf{X}}_k} \mathbf{V}_{\hat{\mathbf{X}}_k}^*$ such that

$$\mathbf{U}_{\hat{\mathbf{X}}_k} = \mathbf{U}_{\mathbf{X}_k} \mathbf{U}_{\hat{\mathbf{S}}_k}, \quad \Sigma_{\hat{\mathbf{X}}_k} = \Sigma_{\hat{\mathbf{S}}_k} \quad \text{and} \quad \mathbf{V}_{\hat{\mathbf{X}}_k} = \mathbf{V}_{\mathbf{X}_{k,2}} \mathbf{V}_{\hat{\mathbf{S}}_k},$$

where $\mathbf{V}_{\mathbf{X}_{k,2}}$ is the submatrix of $\mathbf{V}_{\mathbf{X}_k}$ obtained after removing its first row, i.e. $\mathbf{V}_{\mathbf{X}_k} = \begin{bmatrix} \mathbf{v}_{\mathbf{X}_{k,1}} \\ \mathbf{V}_{\mathbf{X}_{k,2}} \end{bmatrix}$, and $\mathbf{U}_{\hat{\mathbf{S}}_k}$, $\Sigma_{\hat{\mathbf{S}}_k}$ and $\mathbf{V}_{\hat{\mathbf{S}}_k}$ are obtained from the SVD of $\hat{\mathbf{S}}_k = \mathbf{U}_{\hat{\mathbf{S}}_k} \Sigma_{\hat{\mathbf{S}}_k} \mathbf{V}_{\hat{\mathbf{S}}_k}^*$ where

$$\hat{\mathbf{S}}_k = \Sigma_{\mathbf{X}_k} - \mathbf{U}_{\mathbf{X}_k}^* \mathbf{x}_{k-w+1} \mathbf{z}_1^\top \mathbf{V}_{\mathbf{X}_k},$$

and $\mathbf{z}_1 = \begin{bmatrix} 1 & 0 & \cdots & 0 \end{bmatrix}^\top \in \mathbb{R}^w$. Therefore, the SVD of \mathbf{X}_{k+1} is given by $\mathbf{X}_{k+1} = \mathbf{U}_{\mathbf{X}_{k+1}} \Sigma_{\mathbf{X}_{k+1}} \mathbf{V}_{\mathbf{X}_{k+1}}^*$ where

$$\begin{aligned} \mathbf{U}_{\mathbf{X}_{k+1}} &= \mathbf{U}_{\hat{\mathbf{X}}_k} \mathbf{U}_{\hat{\mathbf{S}}_k} = \mathbf{U}_{\mathbf{X}_k} \mathbf{U}_{\hat{\mathbf{S}}_k} \mathbf{U}_{\hat{\mathbf{S}}_k}, \\ \Sigma_{\mathbf{X}_{k+1}} &= \Sigma_{\hat{\mathbf{S}}_k}, \\ \mathbf{V}_{\mathbf{X}_{k+1}} &= \begin{bmatrix} \mathbf{V}_{\hat{\mathbf{X}}_k} \mathbf{V}_{\hat{\mathbf{S}}_k,1} \\ \mathbf{v}_{\hat{\mathbf{S}}_k,2} \end{bmatrix} = \begin{bmatrix} \mathbf{V}_{\mathbf{X}_{k,2}} \mathbf{V}_{\hat{\mathbf{S}}_k} \mathbf{V}_{\hat{\mathbf{S}}_k,1} \\ \mathbf{v}_{\hat{\mathbf{S}}_k,2} \end{bmatrix}. \end{aligned} \tag{7}$$

where $\hat{\mathbf{S}}_k = \begin{bmatrix} \Sigma_{\hat{\mathbf{X}}_k} & \mathbf{U}_{\hat{\mathbf{X}}_k}^* \mathbf{x}_{k+1} \end{bmatrix} = \mathbf{U}_{\hat{\mathbf{S}}_k} \Sigma_{\hat{\mathbf{S}}_k} \mathbf{V}_{\hat{\mathbf{S}}_k}^*$.

Lemma C.2 (Windowed incremental DMD algorithm, Theorem 2 from [4]). Assume that we have access to the following windowed datasets at time t_{k+1}

$$\mathbf{X}_k = \begin{bmatrix} \mathbf{x}_{k-w+1} & \mathbf{x}_{k-w+2} & \cdots & \mathbf{x}_k \end{bmatrix}, \quad \mathbf{Y}_k = \begin{bmatrix} \mathbf{x}_{k-w+2} & \mathbf{x}_{k-w+3} & \cdots & \mathbf{x}_{k+1} \end{bmatrix}.$$

Suppose that at time t_{k+1} , the SVD of $\mathbf{X}_k = \mathbf{U}_{\mathbf{X}_k} \Sigma_{\mathbf{X}_k} \mathbf{V}_{\mathbf{X}_k}^*$ is known, along with the corresponding DMD operator \mathbf{A}_k .

At time t_{k+2} , a new measurement \mathbf{x}_{k+2} is observed, and one can construct the updated datasets

$$\mathbf{X}_{k+1} = \begin{bmatrix} \mathbf{x}_{k-w+2} & \mathbf{x}_{k-w+3} & \cdots & \mathbf{x}_{k+1} \end{bmatrix}, \quad \mathbf{Y}_{k+1} = \begin{bmatrix} \mathbf{x}_{k-w+3} & \mathbf{x}_{k-w+4} & \cdots & \mathbf{x}_{k+2} \end{bmatrix}.$$

Then, at time t_{k+2} , the SVD of \mathbf{X}_{k+1} can be incrementally computed from the known SVD of \mathbf{X}_k using Lemma C.1 and Equation (7). Thus, the DMD operator \mathbf{A}_{k+1} is

$$\mathbf{A}_{k+1} = \mathbf{A}_k + (\mathbf{x}_{k+2} - \mathbf{A}_k \mathbf{x}_{k+1}) \mathbf{v}_{\hat{\mathbf{s}}_{k,2}} \Sigma_{\mathbf{x}_{k+1}}^{-1} \mathbf{U}_{\mathbf{x}_{k+1}}^*.$$

C.1.2 Perturbation theory

Lemma C.3 (Bauer-Fike Theorem [7], Theorem 5.3 from [30]). Let $A \in \mathbb{C}^{n \times n}$ be a diagonalisable matrix and denote by $X = [\mathbf{x}_1, \mathbf{x}_2, \dots, \mathbf{x}_n] \in \mathbb{C}^{n \times n}$ the matrix of its right eigenvectors, where $\mathbf{x}_k \in \mathbb{C}^n$ for $k \in \{1, 2, \dots, n\}$, such that $D = X^{-1}AX = \text{diag}(\lambda_1, \lambda_2, \dots, \lambda_n)$, λ_i being eigenvalues of A , $i \in \{1, 2, \dots, n\}$.

Let $E \in \mathbb{C}^{n \times n}$ be a perturbation of A . Let μ be an eigenvalue of the matrix $A + E \in \mathbb{C}^{n \times n}$, then

$$\min_{\lambda \in \sigma(A)} |\lambda - \mu| \leq \kappa_p(X) \|E\|_p,$$

where $\|E\|_p$ is any matrix p -norm of E , and $\kappa_p(X) = \|X\|_p \|X^{-1}\|_p$ is called the condition number of the eigenvalue problem for matrix A .

Lemma C.4 (Property 5.5 from [30]). Let $A \in \mathbb{C}^{n \times n}$ be a diagonalisable matrix and denote by $X = [\mathbf{x}_1, \mathbf{x}_2, \dots, \mathbf{x}_n] \in \mathbb{C}^{n \times n}$ the matrix of its right eigenvectors, where $\mathbf{x}_k \in \mathbb{C}^n$ for $k \in \{1, 2, \dots, n\}$, such that $D = X^{-1}AX = \text{diag}(\lambda_1, \lambda_2, \dots, \lambda_n)$, λ_i being eigenvalues of A , $i \in \{1, 2, \dots, n\}$.

Let $E \in \mathbb{C}^{n \times n}$ be a perturbation of A with $\|E\|_2 = 1$ and let $A(\varepsilon) = A + \varepsilon E$. Then, the eigenvectors \mathbf{x}_k and $\mathbf{x}_k(\varepsilon)$ of matrices A and $A(\varepsilon)$, with $\|\mathbf{x}_k(\varepsilon)\|_2 = \|\mathbf{x}_k\|_2 = 1$, for $k \in \{1, 2, \dots, n\}$ satisfy

$$\|\mathbf{x}_k(\varepsilon) - \mathbf{x}_k\|_2 \leq \frac{\varepsilon}{\min_{j \neq k} |\lambda_k - \lambda_j|} + \mathcal{O}(\varepsilon^2), \quad \forall k \in \{1, 2, \dots, n\}.$$

C.1.3 Main theoretical result

We prove in the following section Theorem 3.1 which consists of the main theoretical result of our work.

Theorem 3.1 (Upper bound on perturbations of DMD operator eigenvalues and eigenvectors). Consider a p -dimensional stream of observations monitored via Algorithm 1. Let $\mathbf{A} \in \mathbb{C}^{pd \times pd}$ be the DMD operator at time t and let $\tilde{\mathbf{A}} \in \mathbb{C}^{pd \times pd}$ denote the DMD operator at time $t + 1$. Then, there exists a perturbation matrix $\mathbf{E} \in \mathbb{C}^{pd \times pd}$ such that $\tilde{\mathbf{A}} = \mathbf{A} + \mathbf{E}$, where the closed-form of \mathbf{E} is detailed in Appendix C.1. Furthermore, assuming that the DMD operator \mathbf{A} is diagonalisable, then the following results hold:

(i) Eigenvalues (dynamics): let $\tilde{\lambda} \in \sigma(\tilde{\mathbf{A}})$, i.e. $\tilde{\lambda}$ is an eigenvalue of $\tilde{\mathbf{A}}$, then

$$\min_{\lambda \in \sigma(\mathbf{A})} |\tilde{\lambda} - \lambda| \leq \kappa_2(\Phi) \|\mathbf{E}\|_2,$$

where $\|\mathbf{E}\|_2$ denotes the matrix 2-norm of \mathbf{E} , $\kappa_2(\Phi) = \|\Phi\|_2 \|\Phi^{-1}\|_2$ is the condition number of $\Phi \in \mathbb{C}^{pd \times pd}$ and Φ is the eigenvectors matrix of \mathbf{A} .

(ii) Eigenvectors (modes): let $\tilde{\phi}_k \in \mathbb{C}^{pd}$ and $\phi_k \in \mathbb{C}^{pd}$ denote normalised eigenvectors of $\tilde{\mathbf{A}}$ and \mathbf{A} respectively for $k \in \{1, 2, \dots, pd\}$, then

$$\|\tilde{\phi}_k - \phi_k\|_2 \leq \frac{\|\mathbf{E}\|_2}{\min_{j \neq k} |\lambda_k - \lambda_j|} + \mathcal{O}(\|\mathbf{E}\|_2^2), \forall k \in \{1, 2, \dots, pd\}.$$

Proof. At time t , the new datum $x_t \in \mathbb{R}^p$ is observed and one can construct the Hankel batch $\mathcal{X}_t \in \mathbb{R}^{pd \times (w-d+1)}$, with given window length $w \in \mathbb{N}$ and auto-regressive order $d \in \{1, 2, \dots, w\}$, such that

$$\mathcal{X}_t = \begin{array}{c} \overbrace{\mathbf{Y}_t \in \mathbb{R}^{pd \times (w-d)}} \\ \left[\begin{array}{ccccc} x_{t-w+1}^{(1)} & x_{t-w+2}^{(1)} & \cdots & x_{t-d}^{(1)} & x_{t-d+1}^{(1)} \\ x_{t-w+2}^{(1)} & x_{t-w+3}^{(1)} & \cdots & x_{t-d+1}^{(1)} & x_{t-d+2}^{(1)} \\ \vdots & \vdots & \ddots & \vdots & \vdots \\ x_{t-w+d}^{(1)} & x_{t-w+d+1}^{(1)} & \cdots & x_{t-1}^{(1)} & x_t^{(1)} \\ x_{t-w+1}^{(2)} & x_{t-w+2}^{(2)} & \cdots & x_{t-d}^{(2)} & x_{t-d+1}^{(2)} \\ x_{t-w+2}^{(2)} & x_{t-w+3}^{(2)} & \cdots & x_{t-d+1}^{(2)} & x_{t-d+2}^{(2)} \\ \vdots & \vdots & \ddots & \vdots & \vdots \\ x_{t-w+d}^{(2)} & x_{t-w+d+1}^{(2)} & \cdots & x_{t-1}^{(2)} & x_t^{(2)} \\ \vdots & \vdots & \vdots & \vdots & \vdots \\ x_{t-w+1}^{(p)} & x_{t-w+2}^{(p)} & \cdots & x_{t-d}^{(p)} & x_{t-d+1}^{(p)} \\ x_{t-w+2}^{(p)} & x_{t-w+3}^{(p)} & \cdots & x_{t-d+1}^{(p)} & x_{t-d+2}^{(p)} \\ \vdots & \vdots & \ddots & \vdots & \vdots \\ x_{t-w+d}^{(p)} & x_{t-w+d+1}^{(p)} & \cdots & x_{t-1}^{(p)} & x_t^{(p)} \end{array} \right] \in \mathbb{R}^{pd \times (w-d+1)}. \\ \underbrace{\mathbf{X}_t \in \mathbb{R}^{pd \times (w-d)}} \end{array}$$

Recall that our proposed method described in Algorithm 1 consists in applying DMD to snapshots of \mathcal{X}_t . Rigorously, we may define the snapshots of \mathcal{X}_t as its $(w-d+1)$ column vectors, i.e. for $k \in \{t-w+d, t-w+d+1, \dots, t\}$

$$\mathbf{x}_k^\top = \left[x_{k-d+1}^{(1)} \cdots x_k^{(1)} \quad x_{k-d+1}^{(2)} \cdots x_k^{(2)} \cdots x_{k-d+1}^{(p)} \cdots x_k^{(p)} \right] \in \mathbb{R}^{pd}. \quad (8)$$

This leads to defining the lagged snapshots matrices $\mathbf{X}_t \in \mathbb{R}^{pd \times (w-d)}$ and $\mathbf{Y}_t \in \mathbb{R}^{pd \times (w-d)}$ such that

$$\begin{aligned} \mathbf{X}_t &= [\mathbf{x}_{t-w+d} \quad \mathbf{x}_{t-w+d+1} \quad \cdots \quad \mathbf{x}_{t-1}] \in \mathbb{R}^{pd \times (w-d)}, \\ \mathbf{Y}_t &= [\mathbf{x}_{t-w+d+1} \quad \mathbf{x}_{t-w+d+2} \quad \cdots \quad \mathbf{x}_t] \in \mathbb{R}^{pd \times (w-d)}. \end{aligned}$$

Let $\mathbf{A} \in \mathbb{C}^{pd \times pd}$ denote the DMD operator at time t extracted from snapshots matrices \mathbf{X}_t and \mathbf{Y}_t .

Similarly, at time $t + 1$, the new datum $x_{t+1} \in \mathbb{R}^p$ is observed, one can construct $\mathcal{X}_{t+1} \in \mathbb{R}^{pd \times (w-d+1)}$ and using the same notations for the snapshots vectors as in Equation (8), one may obtain

$$\begin{aligned}\mathbf{X}_{t+1} &= [\mathbf{x}_{t-w+d+1} \quad \mathbf{x}_{t-w+d+2} \quad \cdots \quad \mathbf{x}_t] \in \mathbb{R}^{pd \times (w-d)}, \\ \mathbf{Y}_{t+1} &= [\mathbf{x}_{t-w+d+2} \quad \mathbf{x}_{t-w+d+3} \quad \cdots \quad \mathbf{x}_{t+1}] \in \mathbb{R}^{pd \times (w-d)},\end{aligned}$$

along with the corresponding DMD operator at time $t + 1$, denoted by $\tilde{\mathbf{A}} \in \mathbb{C}^{pd \times pd}$.

Applying Lemma C.1 and Lemma C.2 leads to

$$\begin{aligned}\tilde{\mathbf{A}} &= \mathbf{A} + (\mathbf{x}_{t+1} - \mathbf{A}\mathbf{x}_t) \mathbf{v}_{\mathbf{s}_{t,2}} \Sigma_{\mathbf{x}_{t+1}}^{-1} \mathbf{U}_{\mathbf{x}_{t+1}}^* \\ &= \mathbf{A} + \mathbf{E},\end{aligned}$$

where $\mathbf{E} = (\mathbf{x}_{t+1} - \mathbf{A}\mathbf{x}_t) \mathbf{v}_{\mathbf{s}_{t,2}} \Sigma_{\mathbf{x}_{t+1}}^{-1} \mathbf{U}_{\mathbf{x}_{t+1}}^* \in \mathbb{C}^{pd \times pd}$. The matrices $\Sigma_{\mathbf{x}_{t+1}}^{-1}$, $\mathbf{U}_{\mathbf{x}_{t+1}}$ and $\mathbf{v}_{\mathbf{s}_{t,2}}$ are obtained from the SVD of $\mathbf{X}_{t+1} = \mathbf{U}_{\mathbf{x}_{t+1}} \Sigma_{\mathbf{x}_{t+1}} \mathbf{V}_{\mathbf{x}_{t+1}}^*$ using Equation (7).

Under the usual assumption of diagonalisable DMD operators [47], let $\Phi = [\phi_1, \phi_2, \dots, \phi_{pd}] \in \mathbb{C}^{pd \times pd}$ denote the matrix of the right normalised eigenvectors of \mathbf{A} where $\phi_k \in \mathbb{C}^{pd}$ for $k \in \{1, 2, \dots, pd\}$, then Lemma C.3 for the matrix 2-norm implies, for any eigenvalue $\tilde{\lambda}$ of $\tilde{\mathbf{A}}$,

$$\min_{\lambda \in \sigma(\mathbf{A})} |\tilde{\lambda} - \lambda| \leq \kappa_2(\Phi) \|\mathbf{E}\|_2, \quad (9)$$

where $\sigma(\mathbf{A})$ denotes the spectrum of \mathbf{A} and $\kappa_2(\Phi) = \|\Phi\|_2 \|\Phi^{-1}\|_2$ is the condition number of $\Phi \in \mathbb{C}^{pd \times pd}$. Moreover, Lemma C.4 implies that given the normalised eigenvectors $\phi_k \in \mathbb{C}^{pd}$ and $\tilde{\phi}_k \in \mathbb{C}^{pd}$ of \mathbf{A} and $\tilde{\mathbf{A}}$ respectively, $k \in \{1, 2, \dots, pd\}$, then

$$\|\tilde{\phi}_k - \phi_k\|_2 \leq \frac{\|\mathbf{E}\|_2}{\min_{j \neq k} |\lambda_k - \lambda_j|} + \mathcal{O}(\|\mathbf{E}\|_2^2), \forall k \in \{1, 2, \dots, pd\}.$$

□

C.2 Computational complexity

Lemma C.5 (Efficient update of the mean and variance [50]). Consider a univariate time series y_1, y_2, \dots . Let μ_t denote the streaming sample mean and σ_t^2 the streaming sample variance of observations up to time t , i.e. y_1, y_2, \dots, y_t . Then, given initial conditions μ_1 and σ_1^2 , for $t \geq 2$

$$\begin{aligned}\mu_t &= \frac{t-1}{t}\mu_{t-1} + \frac{y_t}{t}, \\ \sigma_t^2 &= \frac{t-1}{t}\sigma_{t-1}^2 + \frac{(y_t - \mu_t)(y_t - \mu_{t-1})}{t}.\end{aligned}$$

Therefore, the sample mean and variance can be sequentially updated with $\mathcal{O}(1)$ time complexity sequentially without having to store all previous observed values.

Lemma C.6 (Computational complexity of DMD defined in Algorithm 2). Given a n -dimensional snapshots matrix $\mathbf{x} = [\mathbf{x}_1, \mathbf{x}_2, \dots, \mathbf{x}_m] \in \mathbb{R}^{n \times m}$ and a fixed SVD rank $r \leq \min(m, n)$, Algorithm 2 extracts the modes $\Phi \in \mathbb{C}^{n \times r}$, the dynamics $\Omega \in \mathbb{C}^{r \times r}$ and the low-rank reconstruction of the inputs $\hat{\mathbf{x}} \in \mathbb{R}^{n \times m}$ with time complexity $\mathcal{O}(mn \cdot \min\{m, n\})$.

Proof. The computational complexity of DMD algorithm is primarily determined by the SVD step, which is performed on the first lagged matrix $\mathbf{X} \in \mathbb{R}^{n \times m}$. The SVD of \mathbf{X} can be performed in two steps [46]: the first one is to reduce \mathbf{X} to a bidiagonal matrix, which can be done in $\mathcal{O}(mn \cdot \min\{m, n\})$ operations; the second one consists in computing the SVD of this new bidiagonal matrix using QR algorithm, which can be done in $\mathcal{O}(\min\{n, m\})$ operations. Therefore, the total cost for the computation of the SVD of \mathbf{X} is $\mathcal{O}(mn \cdot \min\{m, n\})$ since the first step dominates the complexity.

The eigendecomposition of the projected DMD operator $\tilde{\mathbf{A}}_r \in \mathbb{C}^{r \times r}$ can be computed using QR algorithm to obtain all eigenpairs, with a time complexity of $\mathcal{O}(r^3)$. However, one can easily show that $r \leq \min(m, n)$ implies $r^3 \leq mn \cdot \min\{m, n\}$: taking without loss of generality $m \leq n$, i.e. $\min(m, n) = m$, we have $r \leq m$ and thus

$$r^3 \leq m^3 \leq m^2 n = mn \cdot \min(m, n).$$

Therefore, this shows that the eigendecomposition of the projected DMD operator step is dominated by the earlier SVD computation of \mathbf{X} .

The calculation of the pseudo-inverse of $\Phi \in \mathbb{C}^{n \times r}$ relies on the SVD of Φ : indeed, if $\Phi = \mathbf{U}_\Phi \Sigma_\Phi \mathbf{V}_\Phi^*$ where $\mathbf{U}_\Phi \in \mathbb{C}^{n \times n}$, $\Sigma_\Phi \in \mathbb{C}^{n \times r}$ and $\mathbf{V}_\Phi \in \mathbb{C}^{r \times r}$, then $\Phi^\dagger = \mathbf{V}_\Phi \Sigma_\Phi^\dagger \mathbf{U}_\Phi^*$ where Σ_Φ^\dagger is the pseudo-inverse of Σ_Φ obtained by replacing each non-zero diagonal entry by its reciprocal and transposing the resulting matrix. This shows that Φ^\dagger can be estimated in $\mathcal{O}(nr \cdot \min\{n, r\}) = \mathcal{O}(nr^2)$ operations, which is dominated by the complexity of the SVD computation of \mathbf{X} .

Moreover, the reconstruction steps consist of m matrix multiplications, each making $\mathcal{O}(nr)$ operations, hence resulting in the final $\mathcal{O}(mnr)$ time complexity, again dominated by $\mathcal{O}(mn \cdot \min\{m, n\})$.

The adaptive EWMA update steps can be performed with $\mathcal{O}(1)$ complexity as shown in Lemma C.5.

Therefore, Algorithm 2 has $\mathcal{O}(mn \cdot \min\{m, n\})$ time complexity. □

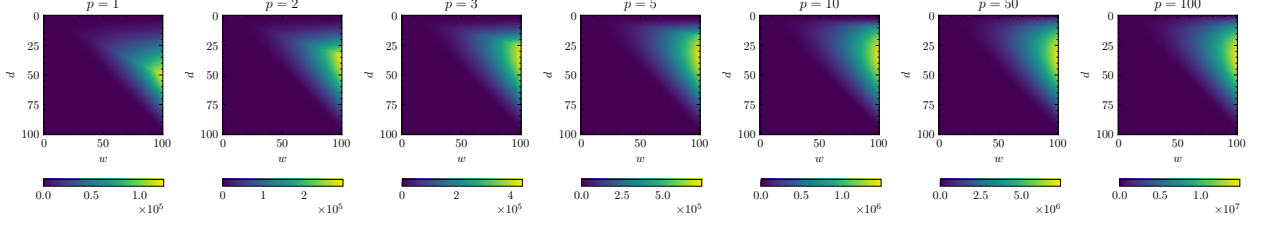


Figure 5: Illustration of $(d, w) \mapsto pd(w - d) \min\{pd, w - d\}$ for different values of p and $1 \leq d \leq w \leq 100$.

Theorem 3.2. The computational complexity of sequence processing steps at each time step t in Algorithm 1 in the context of single changepoint detection is $\mathcal{O}(pd(w - d) \cdot \min\{pd, w - d\})$, where p is the dimension of the input stream, w is the window length and d denotes the auto-regressive order.

Proof. From Algorithm 1, one can notice that at each time step t , the new datum x_t is received and processed to construct the new Hankel batch $\mathcal{X}_t \in \mathbb{R}^{pd \times w - d + 1}$ where p is the input stream dimension, w is the window length and d is the auto-regressive order. The time complexity of these formatting steps is dominated by the DMD step processing \mathcal{X}_t . Applying Lemma C.6, the time complexity of this DMD step on the new Hankel batch is $\mathcal{O}(pd(w - d + 1) \min\{pd, w - d + 1\})$, with $w \in \mathbb{N}$ and $d \in \mathbb{N}, d \leq w$.

- If $pd \leq w - d + 1$, then

$$\mathcal{O}(pd(w - d + 1) \min\{pd, w - d + 1\}) = \mathcal{O}(p^2 d^2 (w - d)).$$

- If $pd > w - d + 1$, i.e. $w - d \leq pd$, then

$$\mathcal{O}(pd(w - d + 1) \min\{pd, w - d + 1\}) = \mathcal{O}(pd(w - d)^2).$$

Lemma C.5 shows that the further adaptive EWMA statistics updates are dominated by the computational complexity of the previous DMD algorithm. Therefore, the time complexity of Algorithm 1 is $\mathcal{O}(pd(w - d) \min\{pd, w - d\})$. □

Corollary C.7 (Computational complexity of hyperparameter selection). During hyperparameter selection as described in Algorithm 3, for any considered model $\theta = \{w, d, r\} \in \Theta$ as defined in Equation (3.5), the total number of operations is maximized when $d = \left\lceil \frac{w}{p+1} \right\rceil$ or $d = \left\lfloor \frac{w}{3} \right\rfloor$ and the worst case time complexity of Algorithm 3 is $\mathcal{O}(pT_0^3)$.

Proof. Assume one monitors a multivariate p -dimensional input stream. Recall that within the hyperparameter selection phase, given a burn-in period T_0 , we consider the set of possible models Θ defined as

$$\Theta := \{(w, d, r) \in \mathbb{N}^3 \mid w \leq T_0, d \leq w, r \leq \min(pd, w - d + 1)\}.$$

Considering that competing model parameters $\theta = (w, d, r) \in \Theta$ may be run in parallel within the burn-period, the time complexity of the complete hyperparameter selection process is equal to the worst case time complexity among all considered models. One may notice that steps within the burn-in period defined in Algorithm 3 have the same time complexity as the one stated in Theorem 3.2. Hence, considering a triplet $\theta = (w, d, r) \in \Theta$,

- (i): $pd \leq w - d$, then $pd(w - d) \cdot \min\{pd, w - d\} = p^2d^2(w - d)$. Assuming fixed window length w , the function $d \mapsto p^2d^2(w - d)$ is maximised for $d = \lceil \frac{2w}{3} \rceil$, i.e. the closest integer to $\frac{2w}{3}$. However, notice that $pd \leq w - d \Leftrightarrow d \leq \frac{w}{p+1}$. Thus, since the function $d \mapsto p^2d^2(w - d)$ is monotonically increasing on $\{1, 2, \dots, \lceil \frac{2w}{3} \rceil\}$, the closest integer on the considered domain of values is $d = \lceil \frac{w}{p+1} \rceil$, and thus $p^2d^2(w - d) \lesssim w^3 \leq T_0^3$.
- (ii): if $pd > w - d$, then $pd(w - d) \cdot \min\{pd, w - d\} = pd(w - d)^2$. For any window length $w \leq T_0$, this cost is maximized for $d = \lceil \frac{w}{3} \rceil$. However, notice that $pd > w - d \Leftrightarrow d > \frac{w}{p+1} \geq \frac{w}{2}$. If $p = 1$, then the closest integer on the domain is $\lceil \frac{w}{2} \rceil$ as in (i), otherwise $d = \lceil \frac{w}{3} \rceil$, and thus $pd(w - d)^2 \lesssim pw^3 \leq pT_0^3$.

□

Consequences. Corollary C.7 leverages Theorem 3.2 result, assuming that competing models can be run in parallel on the burn-in period, to derive a maximum bound of the computational complexity of our proposed model selection procedure. Both results are useful to derive the complexity of our multiple changepoints detection algorithm with hyperparameter selection, described in Algorithm 4, where parameters are adapted automatically after a change is detected with complexity $\mathcal{O}(pT_0^3)$, otherwise the data stream is processed with complexity $\mathcal{O}(pd(w - d) \cdot \min\{pd, w - d\})$ on segments without changes.

D Experiments and simulations

D.1 Computing resources

The experiments were conducted on a high-performance computing cluster, which comprises dual Xeon CPUs with 4 to 10 cores per CPU and 16 to 256 GB of memory per node. The total computation time for the experiments was a couple of hours to 2-3 days for the longest simulations.

D.2 Synthetic data

D.2.1 Data generation process

We consider the following univariate time series generating process

$$x_t = \sum_{k=1}^N \alpha_k \sin(\omega_k t) + \beta t + \gamma + \mathcal{N}(0, \sigma^2), \text{ where}$$

- N denotes the number of periodicities in the dynamics,
- ω_k is the k^{th} periodicity, $k \in \{1, 2, \dots, N\}$,
- α_k corresponds to the amplitude associated to the k^{th} periodicity,
- β denotes a linear trend coefficient,
- γ is the stream location at initialisation,
- σ^2 accounts for the noise variance.

For notational simplicity when considering a single periodicity ($N = 1$), we denote α_1 as α and ω_1 as ω .

The time series are generated for $t \in \{1, 2, \dots, 600\}$ with fixed parameters before and after the changepoint at time $t = \tau = 300$. Periodicities are chosen to avoid discontinuities at the changepoint location that would make the detection of subtle changes in periodicity or amplitude trivial.

We simulate a wide range of change types and magnitudes, covering diverse scenarios to thoroughly assess each algorithm’s performance. The pre-change and post-change process parameters used in the simulations are presented, ensuring a comprehensive exploration of parameter spaces.

Change in periodicity. In this type of change, we consider a single periodicity ($N = 1$), and fix parameters such that $\alpha_1 = 1$, $\beta = 0$, $\gamma = 0$, $\sigma = 0.1$ and the only varying parameter is the periodicity ω , which is chosen such that $\omega = \frac{6\pi}{75}$ when $t < \tau = 300$ and $\omega \in \{\frac{5\pi}{75}, \frac{7\pi}{75}, \frac{8\pi}{75}\}$ when $t \geq \tau = 300$.

Change in location. In this type of change, we consider a single periodicity ($N = 1$), and fix parameters such that $\omega = \frac{4\pi}{75}$, $\alpha = 1$, $\beta = 0$, $\sigma = 0.1$ and the only varying parameter is the location γ , which is chosen such that $\gamma = 0$ when $t < \tau = 300$ and $\gamma \in \{-0.5, 0.5, 1\}$ when $t \geq \tau = 300$.

Change in amplitude. In this type of change, we consider a single periodicity ($N = 1$), and fix parameters such that $\omega = \frac{13\pi}{150}$, $\beta = 0$, $\gamma = 0$, $\sigma = 0.1$ and the only varying parameter is the amplitude α , which is chosen such that $\alpha = 1$ when $t < \tau = 300$ and $\alpha \in \{0.5, 2, 3\}$ when $t \geq \tau = 300$.

Change in trend. In this type of change, we consider a single periodicity ($N = 1$), and fix parameters such that $\omega = \frac{10\pi}{75}$, $\alpha = 1$, $\sigma = 0.1$ and the only varying parameters are the trend β and the location γ , which are chosen such that $\beta = \frac{1}{30}$ and $\gamma = 0$ when $t < \tau = 300$ and $\beta \in \{-\frac{1}{30}, 0, \frac{2}{30}\}$ and $\gamma = 10$ when $t \geq \tau = 300$.

Change in mean. In this type of change, we consider no periodicity ($N = 0$), and fix parameters such that $\beta = 0$, $\sigma = 1$ and the only varying parameter is the location γ , which is chosen such that $\gamma = 0$ when $t < \tau = 300$ and $\gamma \in \{-2, 3, 4\}$ when $t \geq \tau = 300$.

Change in variance. In this type of change, we consider no periodicity ($N = 0$), and fix parameters such that $\beta = 0$, $\gamma = 0$ and the only varying parameter is the noise variance σ , which is chosen such that $\sigma = 0.1$ when $t < \tau = 300$ and $\sigma \in \{0.2, 0.3, 0.4\}$ when $t \geq \tau = 300$.

Change in double periodicity. In this type of change, we consider two periodicities ($N = 2$), and fix parameters such that $\alpha_1 = \alpha_2 = 1$, $\beta = 0$, $\gamma = 0$, $\sigma = 0.1$ and the only varying parameters are the two periodicities ω_1 and ω_2 , which are chosen such that $(\omega_1, \omega_2) = (\frac{9\pi}{75}, \frac{6\pi}{75})$ when $t < \tau = 300$ and $(\omega_1, \omega_2) \in \{(\frac{3\pi}{75}, \frac{5\pi}{75}), (\frac{9\pi}{75}, \frac{3\pi}{75}), (\frac{9\pi}{75}, \frac{4\pi}{75})\}$ when $t \geq \tau = 300$.

D.2.2 Models parameters

In this section, we detail the different methods and parameters that were explored through simulations on synthetic data in Section 4.1. We investigate a variety of parameters across all models, attempting to make the comparison as fair as possible. The burn-in periods (or equivalent parameters) are configured *similarly* for each model to facilitate equivalent initialisations.

CPDMD.

- **Burn-in period** $T_0 = 100$.

As discussed in Section 3.5, the selection of the burn-in period T_0 directly generates the set of possible parameters Θ , defined as

$$\Theta = \{(w, d, r) \in \mathbb{N}^3 \mid w \leq T_0, d \leq w, r \leq \min(pd, w - d + 1)\},$$

where p is the dimension of the input stream. Due to computational constraints, not all triplets can be explored on the burn-in period. We follow the following generation process for Θ which only requires the burn-in period T_0 , and restricts the explored parameters to

- Window length $w \in \{0.4, 0.6, 0.8\} \cdot T_0$,
 - Auto-regressive order $d \in \{0.05, 0.1, 0.2, 0.4\} \cdot T_0$,
 - Truncation rank $r \in 2 \cdot \{1, 2, \dots, p\} = \{2, 4\}$ since $p = 1$.
- **Learning rate** $\lambda = 0.05$ (default), 0.10 of the adaptive EWMA algorithm.
 - **Control limit** $L = 1.5, 2.5, 3.5, 4.5$ (default), 5.5 of the adaptive EWMA algorithm.

mSSA and mSSA-MW. We use the Python implementation provided by the authors of [3] and available via the GitHub repository https://github.com/ArwaAlanqary/mSSA_cpd. We follow the authors guidelines and consider the following parameters:

- **Window size** = 90, 100 (default), 120.
- **Rows** = 3, 7, 10 (default), 13, 15.
- **Distance threshold** = 1, 5 (default), 10.
- **Rank** = 0.95.
- **Training size** = 0.9.

RuLSIF. We use the MATLAB implementation provided by the authors of [52] and available via the GitHub repository https://github.com/aneugithubname/change_detection. While RuLSIF is introduced as a retrospective changepoint detection method, its implementation is analogous to online context, where a threshold needs to be set (and cannot be known in advance) to make online decisions. We follow the authors guidelines and consider the following parameters:

- $n = 25, 50$ (default), 75.
- $k = 5, 10$ (default), 15.
- $\alpha = 0.1$.
- **Threshold** = 0.001, 0.01, 0.05, 1, 2 (default), 3, 4, 5.

BOCPDMS. We use the Python implementation provided by the authors of [20] and available via the GitHub repository <https://github.com/alan-turing-institute/bocpdms>. We consider the same following grid of parameters as in [3]

- **Prior on \mathbf{a}** = 0.01, 1 (default), 100.
- **Prior on \mathbf{b}** = 0.01, 1 (default), 100.
- **Intensity** = 50, 100 (default), 200.

EWMA. We use a self-implementation of the EWMA algorithm introduced by [33] in Python, and we consider the following grid of parameters:

- **Burn-in period** $T_0 = 100$.
- **Learning rate** $r = 0.05$ (default), 0.1.
- **Control limit** $L = 1.5, 2.5$ (default), 3.5, 4.5, 5.5.

EWMVar. We use a self-implementation of the EWMVar algorithm introduced by [26] in Python, and we consider the following grid of parameters:

- **Burn-in period** $T_0 = 100$.
- **Learning rate for the variance** $r = 0.01, 0.05$ (default).
- **Learning rate for the mean** $\lambda = 0.2$.
- **Lower control limit** $C_7 = 0.42, 0.63, 0.68$ (default), 0.91.
- **Upper control limit** $C_8 = 1.08$ (default), 1.12, 1.14, 1.70.

Since all algorithms have different computational complexities, we may run each of them on a different number of sequences. We provide below in Table 3 a summary of the number of sequences that are used for the simulations.

Table 3: Number of sequences used to estimate the performance metrics for each algorithm, change type, and change size.

Sequence length Metrics	Sequences with a single changepoint	Sequences with no changepoint
	$t \in [1, 600]$ Precision, recall, F_1 -Score, ARL_1	$t \in [1, 100000]$ ARL_0
EWMA	1000	100
EWMVar	1000	100
BOCPDMS	50	N/A
RuLSIF	100	10
mSSA	1000	100
mSSA-MW	1000	100
CPDMD	1000	100

Table 4: Summary of selected changepoint detection algorithms capabilities.

Algorithm	Online	Nonparametric	Multivariate data	Periodic data
EWMA	✓	✓	✗	✗
EWMVar	✓	✓	✗	✗
BOCPDMS	✓	✗	✓	✗
RuLSIF	✗	✓	✓	✓
mSSA	✓	✓	✓	✓
mSSA-MW	✓	✓	✓	✓
CPDMD	✓	✓	✓	✓

D.2.3 Global performance

We provide below additional results with BOCPDMS performance for simulations in the context of single changepoint detection. Note that Table 5 is thus the same as Table 1 in Section 4, with only additional performance metrics for the BOCPDMS algorithm.

Table 5: Evaluation of selected changepoint detection algorithms on synthetic data, comparing performance achieved with the parameter set yielding highest F_1 -Score (*best*) against default parametrisation (*default*). We highlight the top two performance metrics for each set of parameters in bold.

Algorithm	Params.	P	R	F_1	ARL_1	ARL_0
EWMA	Best	.669 (.004)	.474 (.003)	.555 (.003)	9.78 (7.44)	71085.25 (41976.94)
	Default	.188 (.003)	.181 (.003)	.185 (.003)	5.88 (5.11)	4261.15 (18156.77)
EWMVar	Best	.275 (.005)	.131 (.002)	.178 (.003)	10.96 (6.86)	71202.77 (45092.24)
	Default	.452 (.009)	.089 (.002)	.148 (.003)	12.36 (7.40)	99900.00 (0.00)
BOCPDMS	Best	.540 (.020)	.319 (.014)	.401 (.016)	4.50 (5.83)	N/A (N/A)
	Default	.492 (.020)	.297 (.013)	.371 (.015)	4.52 (5.96)	N/A (N/A)
RuLSIF	Best	.537 (.013)	.414 (.010)	.468 (.011)	19.01 (6.80)	41934.74 (49177.96)
	Default	.448 (.011)	.364 (.010)	.401 (.010)	23.58 (4.61)	57147.14 (49746.53)
mSSA	Best	.475 (.005)	.266 (.003)	.341 (.004)	6.91 (6.09)	43786.39 (47153.54)
	Default	.304 (.003)	.210 (.002)	.248 (.003)	6.28 (5.80)	27023.57 (42587.84)
mSSA-MW	Best	.443 (.005)	.313 (.004)	.367 (.004)	8.79 (5.87)	13834.54 (32965.67)
	Default	.043 (.001)	.041 (.001)	.042 (.001)	9.11 (7.29)	8210.28 (20999.07)
CPDMD (ours)	Best	.960 (.001)	.902 (.002)	.930 (.002)	7.11 (6.14)	4034.30 (3997.10)
	Default	.978 (.001)	.807 (.003)	.884 (.002)	9.53 (6.47)	58341.28 (38161.07)

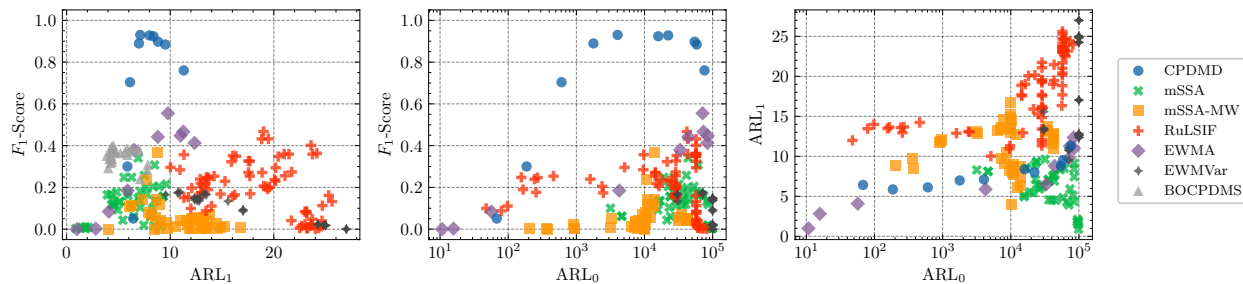


Figure 6: Performance comparison of changepoint detection algorithms on synthetic data across all scenarios. Each dot corresponds to an algorithm with a specific choice of parameter values.

D.2.4 Change in periodicity

The synthetic data generation process for this type of change is detailed in Appendix D.2.1, and we provide in Figure 7 an illustration of this change type and the considered change sizes. The successful detection region corresponds to the time region in which detected changepoints are counted as true positives. With respect to Definition A.4, we use a left margin $\mu_l = 0$ and a right margin $\mu_r = 30$. Performance of the grid of tested models is shown in Figure 8 and a summary of performance is provided in Table 6.

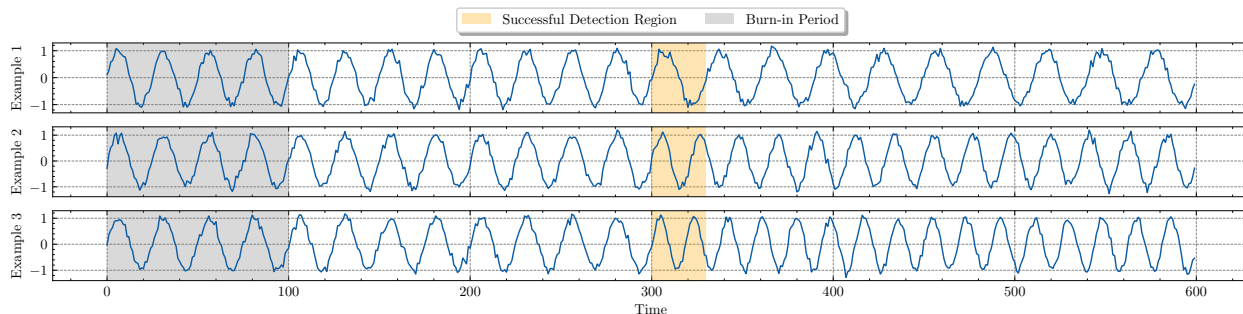


Figure 7: Illustration of the different change sizes considered in the periodicity change simulations.

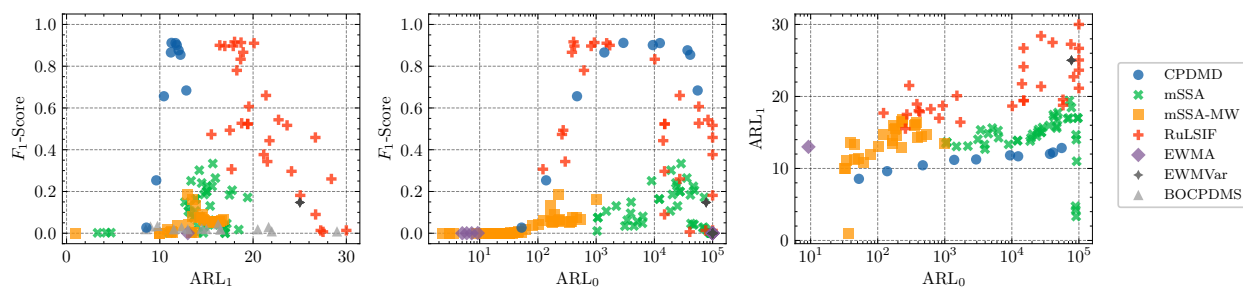


Figure 8: Performance comparison of changepoint detection algorithms on synthetic data for a change in periodicity. Each dot corresponds to an algorithm with a specific choice of parameter values.

Table 6: Evaluation of selected changepoint detection algorithms on synthetic data, comparing performance achieved with the parameter set yielding highest F_1 -Score (*best*) against default parametrisation (*default*). We highlight the top two performance metrics for each set of parameters in bold.

Algorithm	Params.	P	R	F_1	ARL_1	ARL_0
EWMA	Best	.001 (.001)	.001 (.000)	.001 (.000)	13.00 (0.00)	9.27 (0.58)
	Default	.001 (.001)	.001 (.000)	.001 (.000)	13.00 (0.00)	9.27 (0.58)
EWMVar	Best	.297 (.014)	.098 (.005)	.147 (.008)	25.02 (6.45)	77421.77 (35052.88)
	Default	.000 (.000)	.000 (.000)	.000 (.000)	N/A (N/A)	99900.00 (0.00)
BOCPDMS	Best	.121 (.059)	.027 (.014)	.044 (.021)	16.25 (10.21)	N/A (N/A)
	Default	.041 (.024)	.020 (.012)	.027 (.015)	12.33 (7.51)	N/A (N/A)
RuLSIF	Best	.917 (.016)	.917 (.016)	.917 (.016)	18.02 (4.64)	409.30 (411.67)
	Default	.000 (.000)	.000 (.000)	.000 (.000)	N/A (N/A)	99920.00 (0.00)
mSSA	Best	.375 (.010)	.301 (.009)	.334 (.009)	15.68 (5.62)	28707.71 (42667.33)
	Default	.288 (.010)	.188 (.007)	.227 (.008)	15.07 (6.88)	24466.87 (40557.90)
mSSA-MW	Best	.198 (.008)	.178 (.007)	.187 (.007)	12.93 (6.78)	229.29 (207.34)
	Default	.037 (.003)	.037 (.003)	.037 (.003)	11.87 (6.77)	79.18 (65.99)
CPDMD (ours)	Best	.955 (.004)	.872 (.006)	.912 (.005)	11.25 (2.74)	2936.04 (2642.37)
	Default	.994 (.002)	.750 (.008)	.855 (.005)	12.21 (2.56)	41186.52 (35630.17)

D.2.5 Change in location

The synthetic data generation process for this type of change is detailed in Appendix D.2.1, and we provide in Figure 9 an illustration of this change type and the considered change sizes. The successful detection region corresponds to the time region in which detected changepoints are counted as true positives. With respect to Definition A.4, we use a left margin $\mu_l = 0$ and a right margin $\mu_r = 30$. Performance of the grid of tested models is shown in Figure 10 and a summary of performance is provided in Table 7.

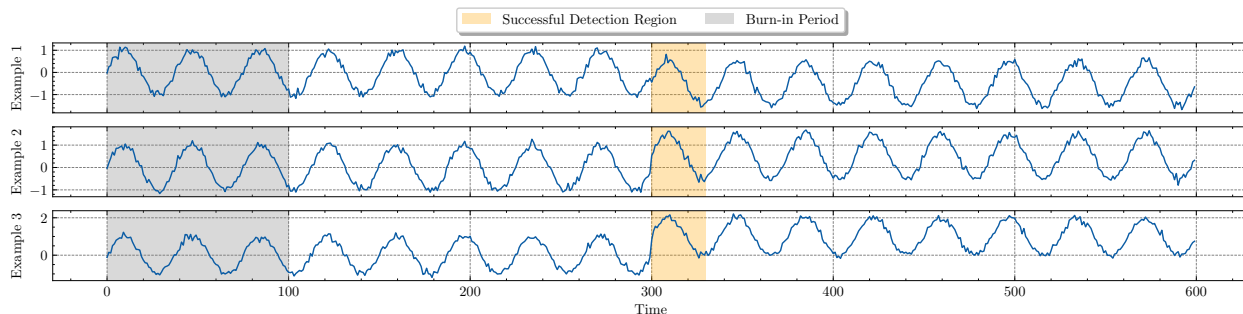


Figure 9: Illustration of the different change sizes considered in the location change simulations.

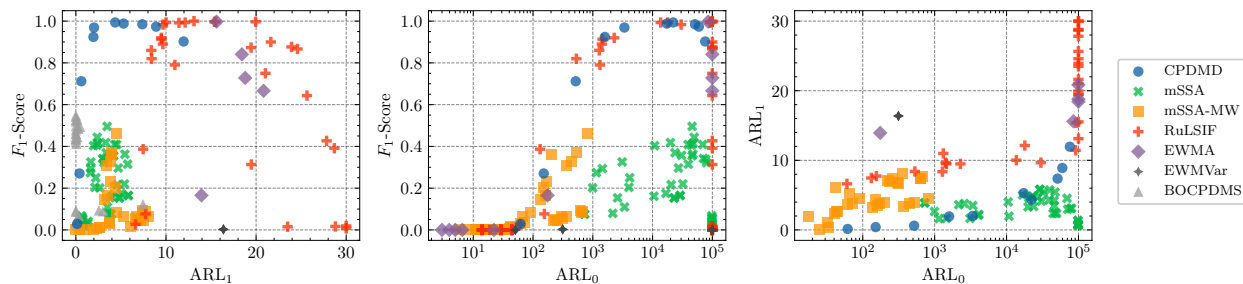


Figure 10: Performance comparison of changepoint detection algorithms on synthetic data for a change in location. Each dot corresponds to an algorithm with a specific choice of parameter values.

Table 7: Evaluation of selected changepoint detection algorithms on synthetic data, comparing performance achieved with the parameter set yielding highest F_1 -Score (*best*) against default parametrisation (*default*). We highlight the top two performance metrics for each set of parameters in bold.

Algorithm	Params.	P	R	F_1	ARL_1	ARL_0
EWMA	Best	.997 (.001)	.997 (.001)	.997 (.001)	15.61 (7.88)	85058.20 (29473.09)
	Default	.000 (.000)	.000 (.000)	.000 (.000)	N/A (N/A)	6.57 (0.50)
EWMVar	Best	.003 (.001)	.003 (.001)	.003 (.001)	16.38 (0.92)	313.45 (33.01)
	Default	.000 (.000)	.000 (.000)	.000 (.000)	N/A (N/A)	99900.00 (0.00)
BOCPDMS	Best	.983 (.017)	.380 (.039)	.548 (.042)	0.00 (0.00)	N/A (N/A)
	Default	.578 (.054)	.320 (.039)	.412 (.044)	0.04 (0.29)	N/A (N/A)
RuLSIF	Best	1.000 (.000)	1.000 (.000)	1.000 (.000)	13.11 (2.57)	99970.00 (0.00)
	Default	.877 (.019)	.877 (.019)	.877 (.019)	23.93 (3.63)	99920.00 (0.00)
mSSA	Best	.771 (.011)	.365 (.009)	.496 (.009)	3.46 (2.48)	45940.81 (46430.82)
	Default	.538 (.012)	.342 (.009)	.418 (.010)	3.31 (2.58)	19904.84 (36828.91)
mSSA-MW	Best	.607 (.011)	.375 (.009)	.464 (.009)	4.56 (3.52)	821.39 (875.52)
	Default	.038 (.004)	.038 (.004)	.038 (.004)	3.74 (5.44)	71.00 (54.03)
CPDMD (ours)	Best	.997 (.001)	.991 (.002)	.994 (.001)	4.37 (6.72)	22104.95 (20841.94)
	Default	.993 (.002)	.955 (.004)	.973 (.002)	8.90 (8.06)	59582.69 (37379.71)

D.2.6 Change in amplitude

The synthetic data generation process for this type of change is detailed in Appendix D.2.1, and we provide in Figure 11 an illustration of this change type and the considered change sizes. The successful detection region corresponds to the time region in which detected changepoints are counted as true positives. With respect to Definition A.4, we use a left margin $\mu_l = 0$ and a right margin $\mu_r = 30$. Performance of the grid of tested models is shown in Figure 12 and a summary of performance is provided in Table 8.

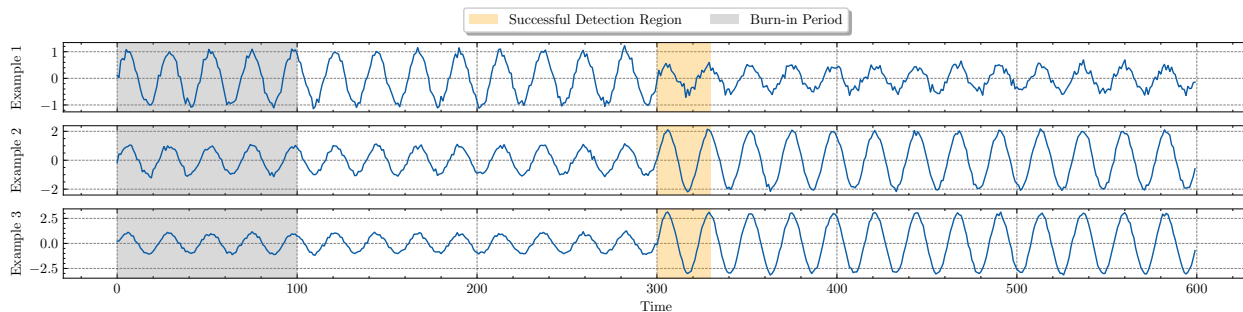


Figure 11: Illustration of the different change sizes considered in the amplitude change simulations.

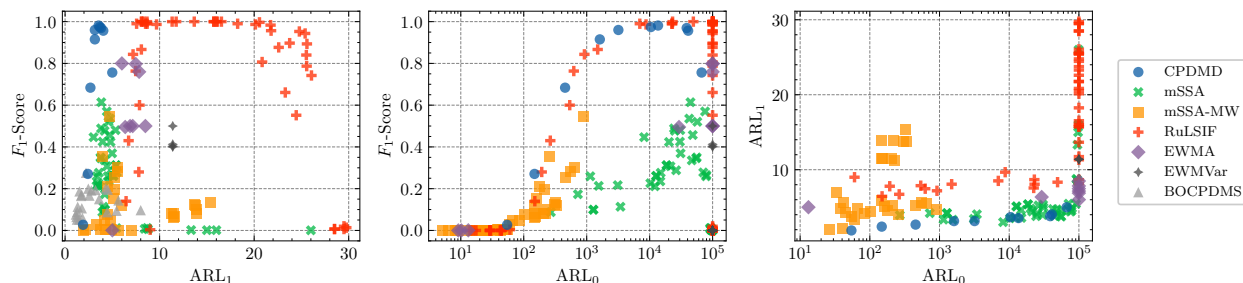


Figure 12: Performance comparison of changepoint detection algorithms on synthetic data for a change in amplitude. Each dot corresponds to an algorithm with a specific choice of parameter values.

Table 8: Evaluation of selected changepoint detection algorithms on synthetic data, comparing performance achieved with the parameter set yielding highest F_1 -Score (*best*) against default parametrisation (*default*). We highlight the top two performance metrics for each set of parameters in bold.

Algorithm	Params.	P	R	F_1	ARL_1	ARL_0
EWMA	Best	1.000 (.000)	.667 (.009)	.800 (.006)	6.01 (1.01)	99900.00 (0.00)
	Default	.567 (.010)	.440 (.009)	.495 (.009)	6.36 (0.97)	29236.98 (39902.66)
EWMVar	Best	1.000 (.000)	.333 (.008)	.500 (.009)	11.39 (1.66)	99900.00 (0.00)
	Default	.000 (.000)	.000 (.000)	.000 (.000)	N/A (N/A)	99900.00 (0.00)
BOCPDMS	Best	.371 (.052)	.220 (.035)	.276 (.041)	2.21 (4.48)	N/A (N/A)
	Default	.206 (.041)	.140 (.029)	.167 (.034)	2.57 (4.34)	N/A (N/A)
RuLSIF	Best	1.000 (.000)	1.000 (.000)	1.000 (.000)	8.06 (2.66)	23118.50 (19393.84)
	Default	.943 (.014)	.943 (.014)	.943 (.014)	25.39 (2.25)	99920.00 (0.00)
mSSA	Best	.813 (.009)	.493 (.009)	.614 (.009)	3.83 (2.01)	44491.10 (45021.24)
	Default	.571 (.011)	.427 (.009)	.489 (.010)	3.80 (2.16)	24336.95 (38369.22)
mSSA-MW	Best	.620 (.010)	.485 (.009)	.544 (.009)	4.70 (2.69)	903.92 (846.10)
	Default	.046 (.004)	.046 (.004)	.046 (.004)	4.14 (5.08)	84.69 (66.65)
CPDMD (ours)	Best	.995 (.001)	.969 (.003)	.981 (.002)	3.55 (1.84)	13587.46 (16750.13)
	Default	.997 (.001)	.920 (.005)	.957 (.003)	4.04 (1.88)	40865.57 (35297.29)

D.2.7 Change in trend

The synthetic data generation process for this type of change is detailed in Appendix D.2.1, and we provide in Figure 13 an illustration of this change type and the considered change sizes. The successful detection region corresponds to the time region in which detected changepoints are counted as true positives. With respect to Definition A.4, we use a left margin $\mu_l = 0$ and a right margin $\mu_r = 30$. Performance of the grid of tested models is shown in Figure 14 and a summary of performance is provided in Table 9.

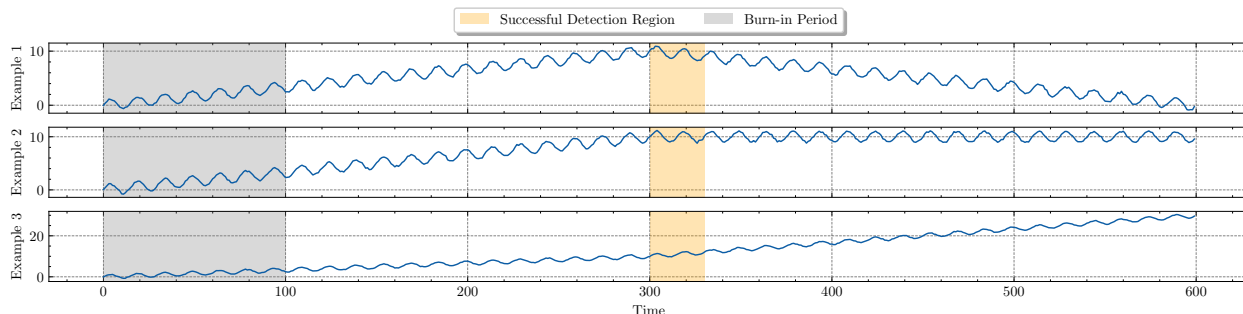


Figure 13: Illustration of the different change sizes considered in the trend change simulations.

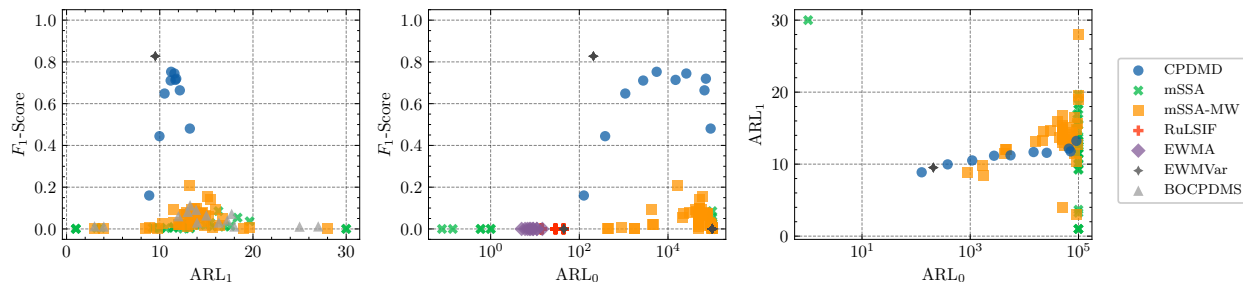


Figure 14: Performance comparison of changepoint detection algorithms on synthetic data for a change in trend. Each dot corresponds to an algorithm with a specific choice of parameter values.

Table 9: Evaluation of selected changepoint detection algorithms on synthetic data, comparing performance achieved with the parameter set yielding highest F_1 -Score (*best*) against default parametrisation (*default*). We highlight the top two performance metrics for each set of parameters in bold.

Algorithm	Params.	P	R	F_1	ARL_1	ARL_0
EWMA	Best	.000 (.000)	.000 (.000)	.000 (.000)	N/A (N/A)	14.67 (1.15)
	Default	.000 (.000)	.000 (.000)	.000 (.000)	N/A (N/A)	7.47 (0.50)
EWMVar	Best	.827 (.007)	.827 (.007)	.827 (.007)	9.52 (5.38)	207.76 (6.63)
	Default	.000 (.000)	.000 (.000)	.000 (.000)	N/A (N/A)	99900.00 (0.00)
BOCPDMS	Best	.194 (.050)	.080 (.022)	.113 (.030)	13.25 (9.43)	N/A (N/A)
	Default	.000 (.000)	.000 (.000)	.000 (.000)	N/A (N/A)	N/A (N/A)
RuLSIF	Best	.000 (.000)	.000 (.000)	.000 (.000)	N/A (N/A)	44.00 (0.00)
	Default	.000 (.000)	.000 (.000)	.000 (.000)	N/A (N/A)	29.00 (0.00)
mSSA	Best	.102 (.006)	.073 (.005)	.085 (.005)	16.30 (7.51)	99880.00 (0.00)
	Default	.033 (.011)	.003 (.001)	.006 (.002)	11.44 (8.19)	99900.00 (0.00)
mSSA-MW	Best	.215 (.007)	.204 (.007)	.210 (.007)	13.15 (5.35)	16158.87 (13911.10)
	Default	.103 (.006)	.082 (.005)	.092 (.005)	13.36 (8.73)	56953.57 (17415.25)
CPDMD (ours)	Best	.907 (.006)	.643 (.009)	.753 (.007)	11.22 (3.73)	5551.77 (4942.42)
	Default	.980 (.003)	.502 (.009)	.664 (.008)	12.15 (3.73)	66510.56 (34645.38)

D.2.8 Change in mean

The synthetic data generation process for this type of change is detailed in Appendix D.2.1, and we provide in Figure 15 an illustration of this change type and the considered change sizes. The successful detection region corresponds to the time region in which detected changepoints are counted as true positives. With respect to Definition A.4, we use a left margin $\mu_l = 0$ and a right margin $\mu_r = 30$. Performance of the grid of tested models is shown in Figure 16 and a summary of performance is provided in Table 10.

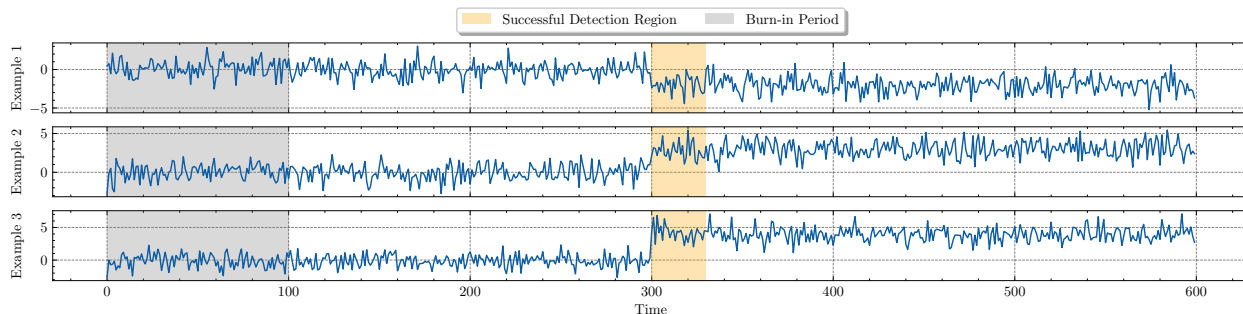


Figure 15: Illustration of the different change sizes considered in the mean change simulations.

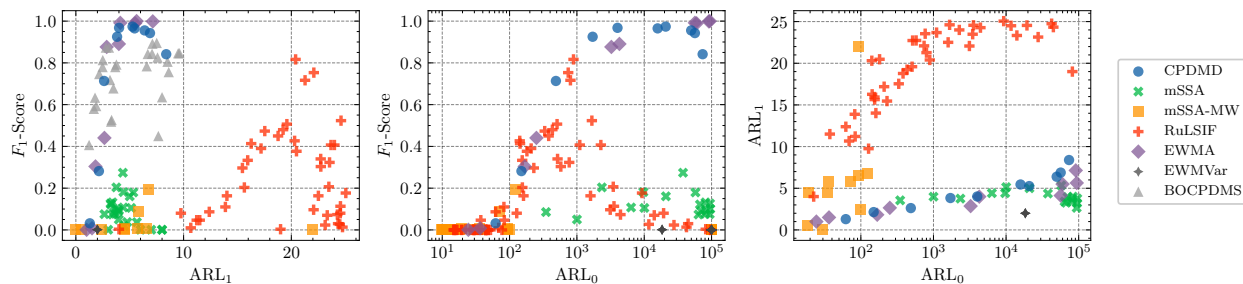


Figure 16: Performance comparison of changepoint detection algorithms on synthetic data for a change in mean. Each dot corresponds to an algorithm with a specific choice of parameter values.

Table 10: Evaluation of selected changepoint detection algorithms on synthetic data, comparing performance achieved with the parameter set yielding highest F_1 -Score (*best*) against default parametrisation (*default*). We highlight the top two performance metrics for each set of parameters in bold.

Algorithm	Params.	P		R		F_1		ARL_1		ARL_0	
EWMA	Best	1.000	(.000)	1.000	(.000)	1.000	(.000)	5.64	(3.42)	94051.07	(21322.11)
	Default	.441	(.009)	.441	(.009)	.441	(.009)	2.65	(1.78)	250.47	(290.29)
EWMVar	Best	.004	(.003)	.001	(.000)	.001	(.001)	2.00	(1.41)	18408.77	(31222.62)
	Default	.000	(.000)	.000	(.000)	.000	(.000)	N/A	(N/A)	99900.00	(0.00)
BOCPDMS	Best	.905	(.024)	.887	(.026)	.896	(.025)	7.50	(5.97)	N/A	(N/A)
	Default	.682	(.040)	.673	(.040)	.678	(.040)	3.48	(3.00)	N/A	(N/A)
RuLSIF	Best	.817	(.022)	.817	(.022)	.817	(.022)	20.40	(3.41)	890.10	(615.54)
	Default	.427	(.028)	.427	(.028)	.427	(.028)	20.30	(5.80)	141.60	(97.35)
mSSA	Best	.480	(.014)	.192	(.007)	.274	(.009)	4.36	(2.66)	37678.13	(45640.53)
	Default	.219	(.009)	.155	(.007)	.181	(.007)	4.41	(3.04)	9717.39	(27538.01)
mSSA-MW	Best	.201	(.008)	.190	(.007)	.196	(.007)	6.73	(6.35)	123.82	(101.40)
	Default	.000	(.000)	.000	(.000)	.000	(.000)	N/A	(N/A)	14.22	(6.40)
CPDMD (ours)	Best	.995	(0.001)	.953	(0.004)	.974	(0.002)	5.26	(4.43)	20833.05	(21516.31)
	Default	.990	(0.002)	.899	(0.006)	.943	(0.003)	6.88	(4.76)	56526.97	(35946.23)

D.2.9 Change in variance

The synthetic data generation process for this type of change is detailed in Appendix D.2.1, and we provide in Figure 17 an illustration of this change type and the considered change sizes. The successful detection region corresponds to the time region in which detected changepoints are counted as true positives. With respect to Definition A.4, we use a left margin $\mu_l = 0$ and a right margin $\mu_r = 30$. Performance of the grid of tested models is shown in Figure 18 and a summary of performance is provided in Table 11.

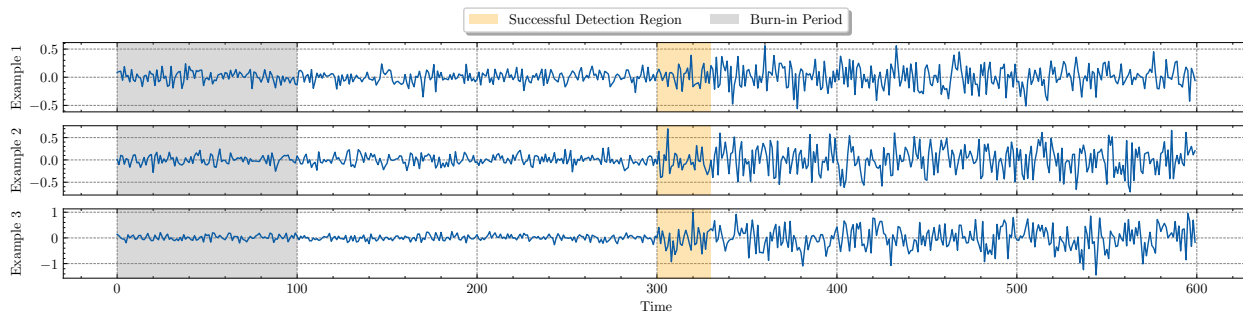


Figure 17: Illustration of the different change sizes considered in the variance change simulations.

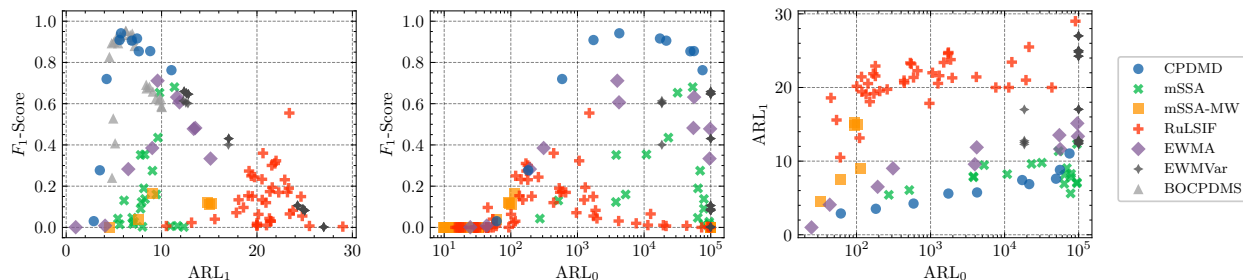


Figure 18: Performance comparison of changepoint detection algorithms on synthetic data for a change in variance. Each dot corresponds to an algorithm with a specific choice of parameter values.

Table 11: Evaluation of selected changepoint detection algorithms on synthetic data, comparing performance achieved with the parameter set yielding highest F_1 -Score (*best*) against default parametrisation (*default*). We highlight the top two performance metrics for each set of parameters in bold.

Algorithm	Params.	P	R	F_1	ARL_1	ARL_0
EWMA	Best	.711 (.009)	.711 (.009)	.711 (.009)	9.58 (7.90)	3959.58 (6248.10)
	Default	.385 (.009)	.385 (.009)	.385 (.009)	9.02 (7.68)	310.69 (373.74)
EWMVar	Best	.704 (.009)	.620 (.009)	.659 (.009)	12.36 (7.40)	99900.00 (0.00)
	Default	.704 (.009)	.620 (.009)	.659 (.009)	12.36 (7.40)	99900.00 (0.00)
BOCPDMS	Best	.953 (.017)	.953 (.017)	.953 (.017)	6.24 (7.10)	N/A (N/A)
	Default	.926 (.022)	.920 (.022)	.923 (.022)	6.96 (7.38)	N/A (N/A)
RuLSIF	Best	.622 (.032)	.500 (.029)	.555 (.029)	23.39 (3.63)	1506.40 (1438.51)
	Default	.301 (.026)	.300 (.026)	.301 (.026)	21.56 (6.98)	179.40 (195.94)
mSSA	Best	.696 (.009)	.665 (.009)	.680 (.008)	11.35 (6.85)	53624.57 (47612.65)
	Default	.354 (.009)	.354 (.009)	.354 (.009)	8.23 (5.97)	10837.83 (28977.50)
mSSA-MW	Best	.164 (.007)	.164 (.007)	.164 (.007)	9.00 (6.13)	113.26 (101.68)
	Default	.000 (.000)	.000 (.000)	.000 (.000)	N/A (N/A)	14.70 (6.44)
CPDMD (ours)	Best	.942 (.004)	.941 (.004)	.941 (.004)	5.75 (5.88)	4244.30 (4398.62)
	Default	.899 (.006)	.815 (.007)	.855 (.006)	8.81 (6.51)	55844.03 (38654.98)

D.2.10 Change in double periodicity

The synthetic data generation process for this type of change is detailed in Appendix D.2.1, and we provide in Figure 19 an illustration of this change type and the considered change sizes. The successful detection region corresponds to the time region in which detected changepoints are counted as true positives. With respect to Definition A.4, we use a left margin $\mu_l = 0$ and a right margin $\mu_r = 30$. Performance of the grid of tested models is shown in Figure 20 and a summary of performance is provided in Table 12.

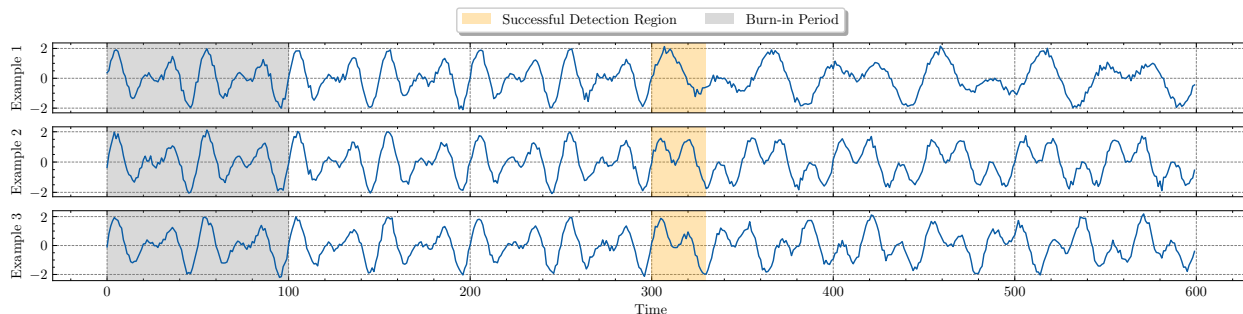


Figure 19: Illustration of the different change sizes considered in the double periodicity change simulations.

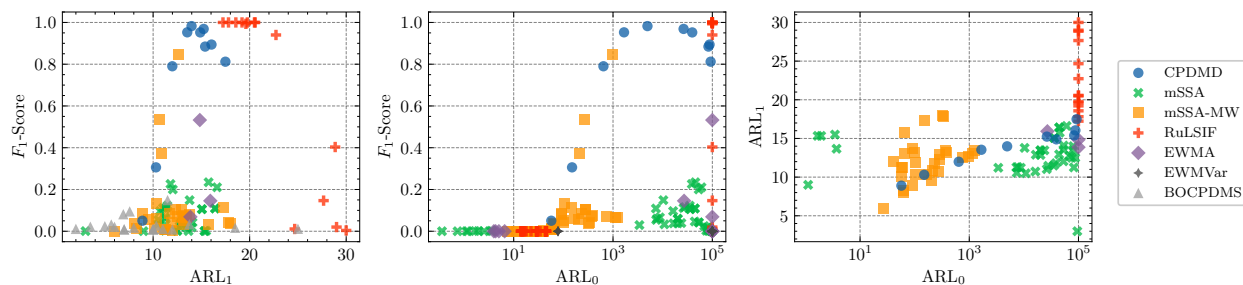


Figure 20: Performance comparison of changepoint detection algorithms on synthetic data for a change in double periodicity. Each dot corresponds to an algorithm with a specific choice of parameter values.

Table 12: Evaluation of selected changepoint detection algorithms on synthetic data, comparing performance achieved with the parameter set yielding highest F_1 -Score (*best*) against default parametrisation (*default*). We highlight the top two performance metrics for each set of parameters in bold.

Algorithm	Params.	P	R	F_1	ARL_1	ARL_0
EWMA	Best	.982 (.004)	.365 (.008)	.533 (.009)	14.84 (2.83)	99900.00 (0.00)
	Default	.000 (.000)	.000 (.000)	.000 (.000)	N/A (N/A)	6.57 (0.50)
EWMVar	Best	.000 (.000)	.000 (.000)	.000 (.000)	N/A (N/A)	99900.00 (0.00)
	Default	.000 (.000)	.000 (.000)	.000 (.000)	N/A (N/A)	99900.00 (0.00)
BOCPDMS	Best	.152 (.030)	.147 (.029)	.149 (.029)	11.50 (10.37)	N/A (N/A)
	Default	.017 (.018)	.007 (.007)	.010 (.009)	10.00 (N/A)	N/A (N/A)
RuLSIF	Best	1.000 (.000)	1.000 (.000)	1.000 (.000)	17.24 (1.55)	99910.00 (0.00)
	Default	.000 (.000)	.000 (.000)	.000 (.000)	N/A (N/A)	99920.00 (0.00)
mSSA	Best	.342 (.012)	.179 (.007)	.235 (.009)	15.75 (4.88)	45381.45 (47480.18)
	Default	.000 (.000)	.000 (.000)	.000 (.000)	9.00 (N/A)	1.12 (0.97)
mSSA-MW	Best	.846 (.007)	.846 (.007)	.846 (.007)	12.67 (4.51)	981.60 (983.34)
	Default	.086 (.005)	.086 (.005)	.086 (.005)	8.86 (3.65)	91.92 (70.20)
CPDMD (ours)	Best	.990 (.002)	.975 (.003)	.983 (.002)	13.98 (5.63)	4938.27 (4722.74)
	Default	.999 (.001)	.809 (.007)	.894 (.004)	16.05 (5.71)	87872.59 (28593.59)

D.3 Real-world experiments

D.3.1 Datasets

In this section, we provide additional details regarding real-world datasets used in Section 4.2.

HASC [16]. Published by the Human Activity Sensing Consortium (HASC), this dataset consists of human activity data recorded via a wearable three-axis accelerometer. Each time series correspond to 120 seconds of acceleration measurements along the x , y , and z axes. The changepoints indicate transitions between six distinct activities: stay, walk, jogging, skip, stair-up, and stair-down. The dataset contains 18 3-dimensional sequences of length $\sim 12,000$. We evaluate performance of selected algorithms on a subset of the HASC dataset made of the first 10 recordings. This sample dataset was provided by the 2011 Human Activity Sensing Consortium challenge and has been previously analysed in changepoint detection studies [3, 24]. This dataset can be downloaded from <http://hasc.jp/hc2011/download-en.html>. Following the definition of F_1 -Score in Appendix 2, and to take into account fluctuations in the human annotations for changepoints locations, we consider a left margin $\mu_l = 50$ and a right margin $\mu_r = 200$.

Digits [51]. The *Optical Recognition of Handwritten Digits Dataset* consists of 8×8 greyscale images (one channel) of a digit. Each pixel corresponds to an integer in the range 0-16. In total, it contains 1,797 samples, leading to ~ 180 digits per class. We generated sequences by concatenating piecewise-constant digit segments, where images were randomly sampled from the original dataset. Each sequence spans a length of 3,000 with approximately 600 timesteps between changepoints. The resulting sequence can be interpreted as a video displaying a single digit that abruptly transitions to a new digit at the changepoints locations. Ultimately, each image is flattened, yielding sequences of length 3,000 with 64 feature dimensions. The original dataset can be downloaded from <https://archive.ics.uci.edu/dataset/80/optical+recognition+of+handwritten+digits>. Following the definition of F_1 -Score in Appendix 2, while the images are extracted from a real-world dataset, we know exactly the changepoint locations and it can be assumed that there is no fluctuation in terms of annotation in this dataset, leading to a left margin $\mu_l = 0$ and a right margin $\mu_r = 50$.

Yahoo [22]. The *S5 - A Labeled Anomaly Detection Dataset* is provided as part of the Yahoo! Webscope program. More specifically, we use the A1 Benchmark which is based on the real production traffic to some of the Yahoo! properties, and consists of 67 univariate time series of length $\sim 1,000$ with seasonalities and trends. Both anomalies and changepoints are labelled by human annotations. This dataset has already been used in the changepoint detection literature [3, 9] to measure performance of algorithms in real-world web traffic data. The dataset can be accessed from <https://webscope.sandbox.yahoo.com/catalog.php?datatype=s&did=70>. Following the definition of F_1 -Score in Appendix 2, and to take into account fluctuations in the human annotations for changepoints locations, we consider a left margin $\mu_l = 50$ and a right margin $\mu_r = 50$.

D.3.2 Models parameters

In this section, we detail the different methods and parameters that were explored through simulations on real-world datasets in Section 4.2. Since each real-world dataset has specific settings (i.e. dimension, sequence length, average inter-changepoint times), we evaluate the performance of each selected algorithm on a grid of parameters which is suited for a given dataset, while trying to make the comparisons as fair as possible and using similar burn-in periods (or equivalent parameters).

Since each considered dataset consists of multiple data streams, we evaluate algorithms' performance via the defined performance metrics (F_1 -Score and covering metric), along with the standard deviation of these performance metrics per set of parameters across all sequences in each dataset.

CPDMD. Given a burn-in period T_0 , we use the same grid generation process as in synthetic data simulations detailed in Section D.2, with explored ranks $r \in 10 \cdot \{1, 2, \dots, p\}$ due to the higher complexity of the generation process of real-world data compared to synthetic data. Note that while increasing the maximum rank, this does not modify the number of explored values for the rank but only consists in increasing the spacing between the explored rank values, and allowing to explore higher values, while avoiding to explore the complete set of possible rank values.

- **Learning rate** $\lambda = 0.05$.
- **Control limit** $L = 2.5, 3.5, 4.5$ (default).
- **HASC dataset**
 - **Burn-in period** $T_0 = 300, 400$ (default).
- **Digits dataset**
 - **Burn-in period** $T_0 = 100, 150$ (default).
- **Yahoo dataset**
 - **Burn-in period** $T_0 = 100, 200$ (default).

mSSA and mSSA-MW. We use the Python implementation provided by the authors of [3] and available via the GitHub repository https://github.com/ArwaAlanqary/mSSA_cpd. We follow the authors guidelines and consider the following parameters:

- **Distance threshold** = 5 (default), 10.
- **Rank** = 0.95.
- **Training size** = 0.9.
- **HASC dataset**

- **Window size** = 300, 400 (default).
- **Rows** = 17, 20 (default).

- **Digits dataset**

- **Window size** = 100, 150 (default).
- **Rows** = 10, 12 (default).

- **HASC dataset**

- **Window size** = 100, 200 (default).
- **Rows** = 10, 14 (default).

RuLSIF. We use the MATLAB implementation provided by the authors of [52] and available via the GitHub repository https://github.com/anevgithubname/change_detection. While RuLSIF is introduced as a retrospective changepoint detection method, its implementation is analogous to online context, where a threshold needs to be set (and cannot be known in advance) to make online decisions. We follow the authors guidelines and consider the following parameters:

- $n = 50$ (default), 75.
- $k = 10$ (default), 15.
- $\alpha = 0.1$.
- **Threshold** = 7.

BOCPDMS. We use the Python implementation provided by the authors of [20] and available via the GitHub repository <https://github.com/alan-turing-institute/bocpdms>. We consider the same following grid of parameters as in [3]

- **Intensity** = 100 (default), 200.
- **Prior on a = Prior on b** = 0.01, 1 (default).

EWMA. We use a self-implementation of the EWMA algorithm introduced by [33] in Python, and we consider the following grid of parameters:

- **Learning rate r** = 0.05 (default), 0.1.
- **Control limit L** = 2.5 (default), 3.5, 4.5.
- **HASC dataset**
 - **Burn-in period T_0** = 300, 400 (default).
- **Digits dataset**

- **Burn-in period** $T_0 = 100, 150$ (default).
- **Yahoo dataset**
 - **Burn-in period** $T_0 = 100, 200$ (default).

EWMVar. We use a self-implementation of the EWMVar algorithm introduced by [26] in Python, and we consider the following grid of parameters:

- **Learning rate for the variance** $r = 0.05$.
- **Learning rate for the mean** $\lambda = 0.2$.
- **Control limits** $(C_7, C_8) = (0.42, 1.7), (0.63, 1.14), (0.68, 1.08)$ (default), $(0.91, 1.12)$.
- **HASC dataset**
 - **Burn-in period** $T_0 = 300, 400$ (default).
- **Digits dataset**
 - **Burn-in period** $T_0 = 100, 150$ (default).
- **Yahoo dataset**
 - **Burn-in period** $T_0 = 100, 200$ (default).

While algorithms like EWMA and EWMVar are designed for univariate changepoint detection, we adapt them to the multivariate datasets (HASC and Digits) by running separate instances per component and taking the union of detected changepoints across all components.

D.3.3 Examples of real-world data segmentations

We provide in Figures 21 and 22 illustrations of CPDMD online changepoint detection results.

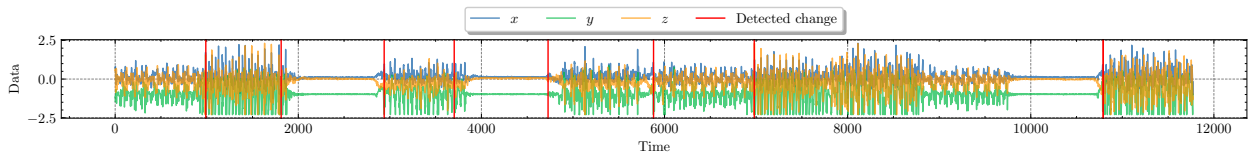


Figure 21: Example of CPDMD online segmentation on a multivariate sequence extracted from the HASC dataset.

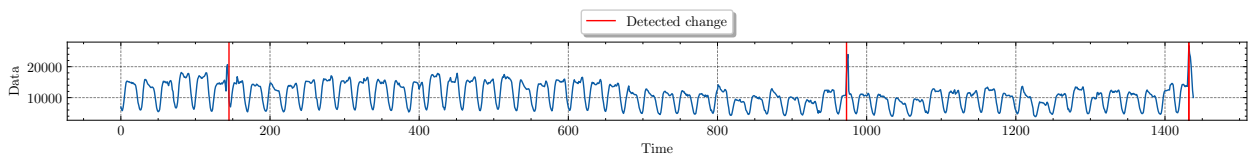


Figure 22: Example of CPDMD online segmentation on a univariate sequence extracted from the Yahoo dataset.

References

- [1] R. P. Adams and D. J. C. MacKay. Bayesian Online Changepoint Detection. *arXiv preprint arXiv:0710.3742*, 2007.
- [2] H. Akaike. A New Look at the Statistical Model Identification. *IEEE Transactions on Automatic Control*, 19(6):716–723, 1974.
- [3] A. Alanqary, A. Alomar, and D. Shah. Change Point Detection via Multivariate Singular Spectrum Analysis. In *Advances in Neural Information Processing Systems*, volume 34, pages 23218–23230, 2021.
- [4] M. Alfatlawi and V. Srivastava. An Incremental Approach to Online Dynamic Mode Decomposition for Time-Varying Systems with Applications to EEG Data Modeling. *Journal of Computational Dynamics*, 7(2):209–241, 2020.
- [5] H. Arbabi and I. Mezic. Ergodic Theory, Dynamic Mode Decomposition, and Computation of Spectral Properties of the Koopman Operator. *SIAM Journal on Applied Dynamical Systems*, 16(4):2096–2126, 2017.
- [6] P. Arbelaez, M. Maire, C. Fowlkes, and J. Malik. Contour Detection and Hierarchical Image Segmentation. *IEEE Transactions on Pattern Analysis and Machine Intelligence*, 33(5):898–916, 2010.
- [7] F. L. Bauer and C. T. Fike. Norms and exclusion theorems. *Numerische Mathematik*, 2(1):137–141, 1960.
- [8] D. A. Bodenham and N. M. Adams. Continuous monitoring for changepoints in data streams using adaptive estimation. *Statistics and Computing*, 27:1257–1270, 2017.
- [9] S. Deldari, D. V. Smith, H. Xue, and F. D. Salim. Time Series Change Point Detection with Self-Supervised Contrastive Predictive Coding. In *Proceedings of the Web Conference 2021*, pages 3124–3135, 2021.
- [10] P. Fearnhead and P. Fryzlewicz. Detecting A Single Change-point. *arXiv preprint arXiv:2210.07066*, 2022.
- [11] P. Fearnhead and Z. Liu. On-line Inference for Multiple Changepoint Problems. *Journal of the Royal Statistical Society Series B: Statistical Methodology*, 69(4):589–605, 2007.
- [12] K. L. Hallgren, A. Heard, N., and M. JM. Turcotte. Changepoint Detection on a Graph of Time Series. *Bayesian Analysis*, 1(1):1–28, 2023.
- [13] P. Héas and C. Herzet. Low-Rank Dynamic Mode Decomposition: An Exact and Tractable Solution. *Journal of Nonlinear Science*, 32(1):8, 2022.
- [14] N. Japkowicz, C. Myers, and M. Gluck. A Novelty Detection Approach to Classification. In *Proceedings of the 14th International Joint Conference on Artificial Intelligence - Volume 1, IJCAI'95*, pages 518–523, San Francisco, CA, USA, 1995. Morgan Kaufmann Publishers Inc.
- [15] T. Kanamori, S. Hido, and M. Sugiyama. A Least-squares Approach to Direct Importance Estimation. *Journal of Machine Learning Research*, 10(48):1391–1445, 2009.

- [16] N. Kawaguchi, N. Ogawa, Y. Iwasaki, K. Kaji, T. Terada, K. Murao, S. Inoue, Y. Kawahara, Y. Sumi, and N. Nishio. HASC Challenge: gathering large scale human activity corpus for the real-world activity understandings. In *Proceedings of the 2nd Augmented Human International Conference*, AH '11, New York, NY, USA, 2011. Association for Computing Machinery.
- [17] Y. Kawahara. Dynamic Mode Decomposition with Reproducing Kernels for Koopman Spectral Analysis. In *Advances in Neural Information Processing Systems*, volume 29. Curran Associates, Inc., 2016.
- [18] Y. Kawahara, T. Yairi, and K. Machida. Change-Point Detection in Time-Series Data Based on Subspace Identification. In *Seventh IEEE International Conference on Data Mining (ICDM 2007)*. IEEE, 2007.
- [19] R. Killick, P. Fearnhead, and I. A. Eckley. Optimal Detection of Changepoints With a Linear Computational Cost. *Journal of the American Statistical Association*, 107(500):1590–1598, 2012.
- [20] J. Knoblauch and T. Damoulas. Spatio-temporal Bayesian on-line changepoint detection with model selection. In *International Conference on Machine Learning*, pages 2718–2727. PMLR, 2018.
- [21] J. N. Kutz, S. L. Brunton, B. W. Brunton, and J. L. Proctor. *Dynamic Mode Decomposition: Data-Driven Modeling of Complex Systems*. Society for Industrial and Applied Mathematics, 2016.
- [22] N. Laptev and S. Amizadeh. Yahoo Anomaly Detection Dataset S5, 2015.
- [23] S. Le Clainche and J. M. Vega. Higher Order Dynamic Mode Decomposition. *SIAM Journal on Applied Dynamical Systems*, 16(2):882–925, 2017.
- [24] S. Liu, M. Yamada, N. Collier, and M. Sugiyama. Change-point detection in time-series data by relative density-ratio estimation. *Neural Networks*, 43:72–83, 2013.
- [25] J. M. Lucas and M. S. Saccucci. Exponentially Weighted Moving Average Control Schemes: Properties and Enhancements. *Technometrics*, 32(1):1–12, 1990.
- [26] J. F. Macgregor and T. J. Harris. The Exponentially Weighted Moving Variance. *Journal of Quality Technology*, 25(2):106–118, 1993.
- [27] D. S. Matteson and N. A. James. A Nonparametric Approach for Multiple Change Point Analysis of Multivariate Data. *Journal of the American Statistical Association*, 109(505):334–345, 2014.
- [28] V. Moskvina and A. Zhigljavsky. An Algorithm Based on Singular Spectrum Analysis for Change-Point Detection. *Communications in Statistics - Simulation and Computation*, 32(2):319–352, 2003.
- [29] E. S. Page. Continuous Inspection Schemes. *Biometrika*, 41(1/2):100–115, 1954.
- [30] A. Quarteroni, R. Sacco, and F. Saleri. *Approximation of Eigenvalues and Eigenvectors*, pages 183–244. Springer Berlin Heidelberg, 2006.

- [31] S. Rabanser, S. Günnemann, and Z. Lipton. Failing Loudly: An Empirical Study of Methods for Detecting Dataset Shift. *Advances in Neural Information Processing Systems*, 32, 2019.
- [32] J. Reeves, J. Chen, X. L. Wang, R. Lund, and Q. Q. Lu. A Review and Comparison of Change-point Detection Techniques for Climate Data. *Journal of Applied Meteorology and Climatology*, 46(6):900–915, 2007.
- [33] S. W. Roberts. Control Chart Tests Based on Geometric Moving Averages. *Technometrics*, 1(3):239–250, 1959.
- [34] G. J. Ross. Parametric and Nonparametric Sequential Change Detection in R: The cpm Package. *Journal of Statistical Software*, 66:1–20, 2015.
- [35] P. J. Rousseeuw. Silhouettes: a graphical aid to the interpretation and validation of cluster analysis. *Journal of Computational and Applied Mathematics*, 20:53–65, 1987.
- [36] P. J. Schmid. Dynamic mode decomposition of numerical and experimental data. *Journal of Fluid Mechanics*, 656:5–28, 2010.
- [37] P. J. Schmid. Dynamic Mode Decomposition and Its Variants. *Annual Review of Fluid Mechanics*, 54(1):225–254, 2022.
- [38] G. Schwarz. Estimating the Dimension of a Model. *The Annals of Statistics*, pages 461–464, 1978.
- [39] A. J. Scott and M. Knott. A Cluster Analysis Method for Grouping Means in the Analysis of Variance. *Biometrics*, pages 507–512, 1974.
- [40] M. Staudacher, S. Telser, A. Amann, H. Hinterhuber, and M. Ritsch-Martel. A new method for change-point detection developed for on-line analysis of the heart beat variability during sleep. *Physica A: Statistical Mechanics and its Applications*, 349(3-4):582–596, 2005.
- [41] M. Sugiyama, T. Suzuki, S. Nakajima, H. Kashima, P. Von Büna, and M. Kawanabe. Direct importance estimation for covariate shift adaptation. *Annals of the Institute of Statistical Mathematics*, 60:699–746, 2008.
- [42] R. Tahmasbi and S. Rezaei. Change Point Detection in GARCH Models for Voice Activity Detection. *IEEE Transactions on Audio, Speech, and Language Processing*, 16(5):1038–1046, 2008.
- [43] N. Takeishi, Y. Kawahara, and T. Yairi. Learning Koopman Invariant Subspaces for Dynamic Mode Decomposition. *Advances in Neural Information Processing Systems*, 30, 2017.
- [44] R. L. Thorndike. Who belongs in the family? *Psychometrika*, 18(4):267–276, 1953.
- [45] M. K. Titsias, J. Sygnowski, and Y. Chen. Sequential changepoint detection in neural networks with checkpoints. *Statistics and Computing*, 32(2):26, 2022.
- [46] L. N. Trefethen and D. Bau. *Numerical Linear Algebra*. SIAM, 2022.
- [47] J. H. Tu, C. W. Rowley, D. M. Luchtenburg, S. L. Brunton, and J. N. Kutz. On dynamic mode decomposition: Theory and applications. *Journal of Computational Dynamics*, 1(2):391–421, 2014.

- [48] R. Turner, Y. Saatci, and C. E. Rasmussen. Adaptive Sequential Bayesian Change Point Detection. In *Temporal Segmentation Workshop at NIPS*, pages 1–4, 2009.
- [49] G. J. J. Van den Burg and C. K. I. Williams. An Evaluation of Change Point Detection Algorithms. *arXiv preprint arXiv:2003.06222*, 2020.
- [50] B. P. Welford. Note on a Method for Calculating Corrected Sums of Squares and Products. *Technometrics*, 4(3):419–420, 1962.
- [51] L. Xu, A. Krzyzak, and C. Y. Suen. Methods of Combining Multiple Classifiers and Their Applications to Handwriting Recognition. *IEEE Transactions on Systems, Man, and Cybernetics*, 22(3):418–435, 1992.
- [52] M. Yamada, T. Suzuki, T. Kanamori, H. Hachiya, and M. Sugiyama. Relative Density-Ratio Estimation for Robust Distribution Comparison. In *Advances in Neural Information Processing Systems*, volume 24, 2011.